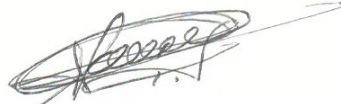


TESIS DEFENDIDA POR

Varun Katare

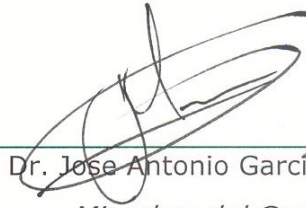
Y APROBADA POR EL SIGUIENTE COMITÉ



Dr. Jaime Sánchez García
Director del Comité



Dr. Jose Rosario Gallardo López
Miembro del Comité



Dr. Jose Antonio García Macias
Miembro del Comité



Dr. Arturo Velázquez Ventura
Miembro del Comité



Dr. Luis Armando Villaseñor González
Miembro del Comité



Dr. Arturo Velázquez Ventura
*Coordinador del programa de
posgrado en Electrónica y
Telecomunicaciones*



Dr. Edgar Gerardo Pavía López
Director de Estudios de Posgrado

2 de Agosto de 2007

THESIS DEFENDED BY

Varun Katare

AND APPROVED BY FOLLOWING COMMITTEE



Dr. Jaime Sánchez García
Committee Director



Dr. Jose Rosario Gallardo López
Committee Member



Dr. Jose Antonio García Macias
Committee Member



Dr. Arturo Velázquez Ventura
Committee Member



Dr. Luis Armando Villaseñor González
Committee Member



Dr. Arturo Velázquez Ventura
*Electronics and Telecommunication
Postgraduate program Coordinator*



Dr. Edgar Gerardo Pavía López
Postgraduate Studies Director

2nd of August, 2007

**CENTRO DE INVESTIGACIÓN CIENTÍFICA Y DE EDUCACIÓN SUPERIOR
DE ENSENADA**



**PROGRAMA DE POSGRADO EN CIENCIAS
EN ELECTRÓNICA Y TELECOMUNICACIONES**

MODELO DE CANAL RADIO PARA REDES DE SENSORES INALAMBRICOS

TESIS

que para cubrir parcialmente los requisitos necesarios para obtener el grado de
MAESTRO EN CIENCIAS

Presenta:

VARUN KATARE

Ensenada, Baja California, México, Agosto 2007

RESUMEN de la tesis de **Varun Katare**, presentada como requisito parcial para la obtención del grado de MAESTRO EN CIENCIAS en Electrónica y Telecomunicaciones. Ensenada, Baja California, México. Agosto 2007.

MODELO DE CANAL RADIO PARA REDES DE SENSORES INALÁMBRICOS

Resumen aprobado por:

Dr. Jaime Sánchez García

El uso de redes de sensores inalámbricos ha ganado más y más fama cada día por su simplicidad, tamaño reducido, bajo costo y eficiencia en potencia. Pero sin embargo, para hacer posible la implementación de una red de sensores inalámbricos es necesario comprender el comportamiento del canal de radio del medio en el que será implementado. Esto es, comprender cómo viajará la señal a través del canal de radio, por ejemplo, cómo será la pérdida de potencia, la respuesta a impulso, el retraso en la velocidad, etc. Por esto, para poder estudiar el comportamiento del canal de radio para WSN (red de sensores inalámbricos), es necesario desarrollar un modelo de canal de radio que proporcione los parámetros mencionados.

Existen muchos modelos diseñados para diferentes medios y bandas de frecuencia pero ninguno de ellos diseñado específicamente para WSN. Como WSN utiliza sensores que trabajan con una banda de frecuencia de 2.4GHz, usando el estándar IEEE 802.15.4 con una potencia bastante baja, etc. se vuelve necesario un modelo de canal de radio diseñado específicamente para una mejor implementación y eficiencia de red.

Esta tesis propone el primer modelo estadístico de canal de radio para WSN en un medio cerrado, el modelo diseñado nos proporciona la respuesta de impulso del canal, el perfil de pérdida de potencia, pérdida de rms y pérdida de exceso. Esta tesis también provee los resultados obtenidos por mediciones físicas y un modelo determinado para los perfiles de cobertura y pérdida de potencia, que ayudan en la implementación de WSN.

Palabras clave: red de canales inalámbricos, modelo de canal de radio, 2.4GHz, IEEE 802.15.4, modelo estadístico.

ABSTRACT of the thesis presented by **Varun Katare** as a partial requirement to obtain the **MASTER OF SCIENCE** degree in **ELECTRONICS AND TELECOMMUNICATIONS**. Ensenada, Baja California, Mexico. August 2007.

RADIO CHANNEL MODEL FOR WIRELESS SENSOR NETWORK

The use of wireless sensor network has been gaining more and more acceptance everyday because of its simplicity, small size, low cost and power efficiency. But still in order to implement a wireless sensor network there is a need to understand the radio channel behavior of the environment in which it would be implemented. By this it means how the signal would travel in the radio channel, for example how would be the power decay, impulse response, delay spread, etc. Hence in order to study the radio channel behavior for WSN it is necessary to develop a radio channel model providing with the above mentioned channel parameters.

There are many designed models for different environments and different frequency bands but none of them is specifically designed for WSN. As WSN uses sensors that work in the 2.4 GHz frequency band, using the IEEE 802.15.4 standard at very low power, etc., this results in needing a radio channel model specifically designed for WSN, for better network implementation and efficiency.

This thesis first adapts a statistical radio channel model for WSN for indoor environment, the designed model provides us with the channel impulse response, power decay profile, rms delay and excess delay. This thesis also provides the results obtained from the physical measurements and a deterministic model for the coverage and power decay profile which helps in the implementation of WSN.

Keywords: wireless sensor network, radio channel model, 2.4 GHz, IEEE 802.15.4, statistical model.

*I dedicate this thesis to my loving girlfriend **Diana**.*

Acknowledgments

This thesis would not have been possible without the support of many people. Many thanks to my adviser, **Dr. Jaime Sánchez García**, who read my numerous revisions and helped in making some sense of the confusion. Also thanks to my committee members, **Dr. Arturo Velázquez Ventura, Dr. Jose Rosario Gallardo López, Dr. Luis A. Villaseñor González, Dr. Jose Antonio García Macías**, who offered guidance and support. Thanks to **CICESE** for providing me with acceptance as a student, and Government of **India** and **México** for providing me with the financial means to complete this thesis.

A **special** thanks goes for great support that I got from my great loving girlfriend **Diana**, who always stood by my side for all kinds of problems that I faced during the two years of my Masters.

I would also like to convey my thanks to my parents **Shobha Katare** and **O.P. Katare** and sister **Shruti Katare** for their patience, love and support in all respects.

Thanks to **girlfriend's family** who always treated me with lot of love and affection and never made me realize that I am so far away from home. Their support and friendship made these two years pass really fast and joyable.

Finally would like to thank all my friends who helped me by all means to finish my thesis and my exciting two years stay in Mexico. Thanks to my friends Carlos, Paul, Javier, Marco, Sergio, Andrés, Alejandro, Jorge, Kobe, Rodolfo, Iván, Rogelio, Tuzo, Ariel, Dania, Edna, Richard, Rubén, Aldo, Beto, Danny boy, Saraí and Luis for their love and friendship.

Thanks to first two people I met from CICECE, who always kept my enthusiasm high by their encouraging smile, the secretaries Rosa Carolina and Martha Aurora.

RESUMEN EJECUTIVO

MODELO DE CANAL RADIO PARA REDES DE SENSORES INALAMBRICOS

El uso de redes de sensores inalámbricas ha ganado más y más popularidad cada día por su simplicidad, reducido tamaño, bajo costo y eficiente consumo de potencia. Sin embargo, para hacer posible la implementación de una red de sensores inalámbricas es necesario comprender el comportamiento del canal radio en el medio en el que será implementado. Esto es, comprender cómo viajará la señal a través del canal de radio, por ejemplo, cómo será la pérdida de potencia, la respuesta al impulso, el retardo en la propagación, etc. Por esto, para poder estudiar el comportamiento del canal de radio para WSN (red de sensores inalámbrica), es necesario desarrollar un modelo de canal radio que proporcione los parámetros mencionados.

Existen muchos modelos diseñados para diferentes medios y bandas de frecuencia pero ninguno de ellos diseñado específicamente para WSN. Como WSN utiliza sensores que trabajan con una banda de frecuencia de 2.4GHz, usando el estándar IEEE 802.15.4 con una potencia bastante baja, se vuelve necesario un modelo de canal de radio diseñado específicamente para una mejor implementación y eficiencia de la red.

Esta tesis propone el primer modelo estadístico de canal de radio para WSN en un medio cerrado, el modelo diseñado nos proporciona la respuesta al impulso del canal, el perfil de pérdida de potencia, pérdida rms y pérdida de exceso. Esta tesis también provee los resultados obtenidos por mediciones físicas y un modelo determinado para los perfiles de cobertura y pérdida de potencia, que ayudan en la implementación de WSN.

Palabras clave: red de sensores inalámbrica, modelo de canal de radio, 2.4GHz, IEEE 802.15.4, modelo estadístico.

I. Introducción

El objetivo principal de esta tesis es diseñar un modelo de canal radio para redes de sensores inalámbricas para ambientes interiores, que trabaje con una frecuencia de 2.4 GHz. Este objetivo incluye también la implementación de una red con Sky-tmotes, que están diseñados en base al estándar IEEE 802.15.4, en el segundo piso del edificio de Física Aplicada de CICESE y analizar las variaciones de cobertura y potencia en ambientes reales.

La propuesta de modelo de canal radio, motivo de esta tesis, consiste en tres partes:

1. La primera corresponde a un modelo estadístico de canal, que ofrece información básica del comportamiento de canal de radio, como respuesta al impulso, llegada de clusters y rayos, retraso excesivo, retraso de *root mean square (RMS)* y el perfil de pérdida de potencia, ayudando enormemente a alcanzar un mejor entendimiento del comportamiento del canal. Los resultados de simulación de matlab son presentados en esta tesis para apoyar este objetivo. Este puede considerarse como una primera aproximación al modelo de canal de radio para WSN, ya que existen algunos modelos (utilizados por varias compañías fabricantes de sensores), que solo utilizan la pérdida por trayectoria entre dos sensores; este modelo es incompleto ya que no provee mas detalles del canal de radio (v.g. desvanecimientos por multitrayectorias).
2. La segunda parte utiliza un modelo determinístico diseñado específicamente para el 2do. piso de física aplicada, basado en el número de reflexiones, precisión de ángulo y límite de potencia. El modelo muestra la cobertura de un sensor y la

cobertura lograda al combinar diferentes sensores; y da una descripción de la pérdida de potencia, lo que podría ayudar a implementar redes de sensores eficientes en en cuanto a cobertura. También considera en detalle las medidas de cada elemento del piso (paredes, puertas, ventanas, etc.) y cada estructura junto con la permitividad y conductividad de los diferentes materiales.

3. Finalmente, se toman lecturas físicas de cobertura y potencia entre motes programándolos para transmitir continuamente y con la ayuda de un analizador de espectro de 2.4GHz. Los resultados en los tres casos fueron comparados para entender y concluir sobre el comportamiento del canal de radio para interiores.

II. Medición física

Todas las mediciones físicas para la potencia y cobertura se tomaron, en el segundo piso del edificio de física aplicada de CICESE (figura-1), usando sensores sky tmote y un analizador de espectros de 2.4GHz. Se tomaron series de lecturas con el sensor y el analizador de espectro fijos colocados en la parte superior de la esquina derecha del piso y moviendo el sensor emisor a diferentes lugares, utilizando finalmente el promedio de lecturas como se puede ver en la siguiente figura que representa la estructura arquitectónica del piso.

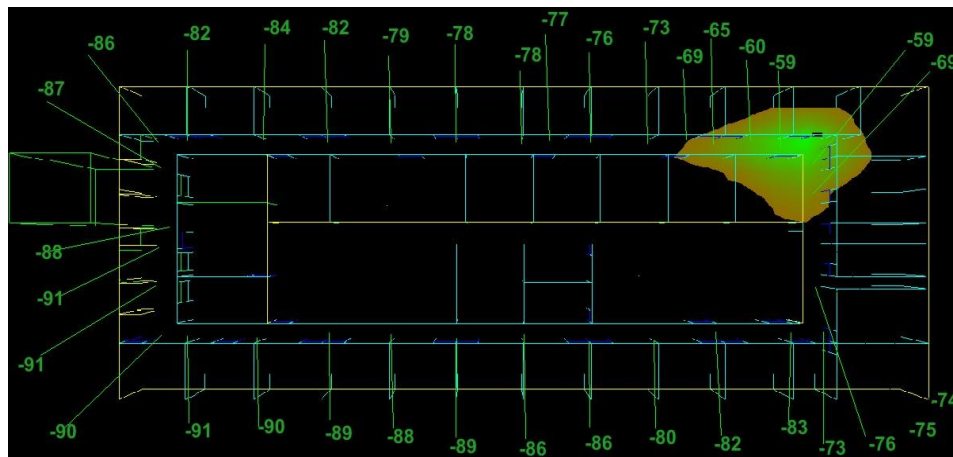


Figura 1: Medida de la potencia recibida (dBm) en el segundo piso del edificio de Física Aplicada, CICESE.

El rango de potencia en el que se mantiene conectividad entre dos sensores varía de -59dBm a -87dBm, mas allá de -87dBm aún se reciben lecturas de potencia hasta -91dBm pero no hay conectividad entre sensores.

La figura 2 describe la variación de potencia en el 2do piso de F.A. para línea de vista (LOS) :

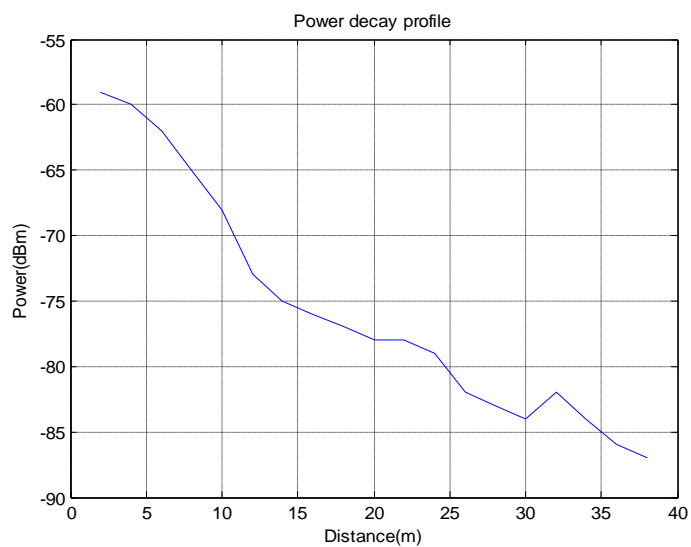


Figura 2: Potencia recibida (dBm) vs. distancia (m)

III. Modelo estadístico

III.1 Modelo de referencia

El modelo de referencia utilizado para diseñar el modelo estadístico de canal de radio es el modelo Saleh-Valenzuela (S-V). Saleh y Valenzuela obtuvieron los resultados de sus mediciones en edificios de tamaño mediano de dos pisos y desarrollaron una simulación de modelo de canal de radio para interiores analizando varios esquemas de comunicación. El modelo congenió con las mediciones y puede utilizarse para otros edificios ajustando sus parámetros [Saleh & Valenzuela, 1987]. El modelo asume que:

1. Los componentes multitrayectoria llegan en clusters.
2. La amplitud recibida de cada componente es una variable aleatoria Raleigh independiente cuya varianza disminuye exponencialmente con el retardo de propagación de cada cluster.
3. Los ángulos de fase correspondientes para cada componente son variables aleatorias independientes, con densidad uniforme sobre $[0, 2\pi]$.
4. Los clusters y las componentes multitrayectoria dentro de cada cluster forman un proceso de Poisson con tasas de arribo diferentes.
5. Las componentes multitrayectoria y los clusters tienen tiempos de inter-arribo distribuidos exponencialmente.
6. La formación de clusters se relaciona con la estructura del edificio, mientras que las componentes multitrayectorias de cada cluster se forman por reflexiones múltiples sobre objetos en el área del transmisor y receptor.

El modelo es suficientemente flexible para adaptarse con buena precisión a la respuesta del canal medida y suficientemente simple para simulación. Este modelo es exitoso para aplicarlo en ambientes de oficina pero su implementación en industria y ambientes exteriores no es tan exitosa. La razón es que el ambiente en industria y exteriores es inherentemente diferente y la propagación depende completamente del ambiente.

Hay cinco parámetros clave que definen el modelo de canal multitrayectoria S-V que son básicos en el diseño de un modelo de canal radio:

- 1) Λ el índice de llegada de clusters
- 2) λ índice de llegada de rayos, p.e. el índice de llegada de trayectoria en cada cluster
- 3) Γ el factor de disminución exponencial de cluster
- 4) γ el factor de disminución exponencial de rayo
- 5) σ_a la desviación estándar del término desvaneciente lognormal (dB).

El modelo multitrayectoria Saleh-Valenzuela es dado por la respuesta al impulso en tiempo discreto:

$$\boxed{h(t) = \sum_{l=1}^L \sum_{k=1}^{K_l} \alpha_{k,l} e^{-j2\pi f_c t} e^{j2\pi f_c \tau_{k,l}} e^{-\gamma t} e^{-\Gamma l} e^{j\phi_{k,l}} \quad (1)}$$

Donde:

L = número de clusters;

K_l = número de componentes multitrayectoria (MPC) o rayos en el cluster l_{th} ;

$\alpha_{k,l}$ = coeficiente multitrayectoria del rayo k_{th} en el cluster l_{th} ;

T_l = tiempo de llegada del primer rayo del cluster l_{th} ;

$\tau_{k,l}$ = retraso del rayo k_{th} en el cluster l_{th} relativo al tiempo de llegada de la primera trayectoria.

Los clusters y rayos forman un proceso de llegada Poisson con distribuciones dadas por:

$$P(T_l/T_{l-1}) = \Lambda \exp(-\Lambda(T_l - T_{l-1})), l > 0 \quad (2)$$

$$p(\tau_{k,l}/\tau_{(k-1),l}) = \lambda \exp(-\lambda(\tau_{k,l} - \tau_{(k-1),l})), k > 0 \quad (3)$$

Donde: Λ = tasa de arribo de clusters; λ = tasa de arribo de rayos.

Aquí se asume que todos los clusters tienen la misma tasa de arribo de rayos, de cualquier modo, algunas mediciones indican que la tasa de llegada es mayor para los clusters que llegan más tarde.

III.2. Modelo estadístico diseñado

III.2.1 Path loss

El cálculo de la potencia recibida debe proceder del siguiente modo:

- 1) Como primer paso, tiene que definirse el espectro de potencia transmitido $P_t(f)$ que será visto “al aire”.

Este espectro es el producto del espectro de salida del amplificador transmisor

$P_{TX-amp}(f)$ por la eficiencia de antena dependiente de la frecuencia $\eta_{rx-ant}(f)$.

$$P_r(f) = P_{TX-amp}(f) \eta_{rx-ant}(f) \quad (7)$$

De [Kadel & Lorenz, 1995] y [Rossi, 1999] *pérdida por trayectoria* puede describirse mejor como función de la frecuencia así como de la distancia, de acuerdo a la ecuación 8.

$$P(d, f) = P_L(d) + P_F(f) \quad (8)$$

La dependencia en frecuencia de la *pérdida por trayectoria* está dada como [Qui & Lu, 1996]

$$\sqrt{P_F(f)} \propto f^k \quad (9)$$

Donde k depende de la frecuencia y la *pérdida por trayectoria dependiente* de la distancia en dB se describe como:

$$P_L(d) = PL_0 + 10n \log\left(\frac{d}{d_0}\right) \quad (10)$$

Donde la distancia de referencia (d_0) se fija a 1m y PL_0 es el *pérdida por trayectoria* a la distancia de referencia, n es el exponente de *pérdida por trayectoria* que depende del medio, para LOS en interiores es 1 en el pasillo y prácticamente 2 en ambientes de oficina y para NLOS varía de 3 a 4 [U.C.A.N., 2003].

2) En el siguiente paso, usando las ecuaciones 8, 9 y 10, se calcula la densidad de potencia dependiente de la frecuencia, a una distancia d ,

$$\hat{P}(f, d) = \frac{P(d, f)}{A_{RX}} \quad (11)$$

Donde f_c es la frecuencia de referencia, la constante de normalización K_0 se determinará luego y $n=2$.

3) Finalmente, se determina la potencia recibida dependiente de la frecuencia $P_r(d, f)$, multiplicando la densidad de potencia $\hat{P}(f, d)$ en la posición del receptor con el área de antena A_{RX}

$$A_{eff} = \frac{\lambda^2 G_{RX}}{4\pi} \quad (12)$$

donde G_{RX} es la ganancia de antena del receptor; y también multiplicando por la eficiencia de antena $\eta_{RX-ant(f)}$. Como se asume nuevamente que la radiación se promedia con todos los ángulos incidentes, la ganancia de antena es unitaria, independiente de la frecuencia considerada. La potencia recibida dependiente de la frecuencia se da nuevamente por:

$$P_r = P_t \frac{A_{eff}}{4\pi r^2} \quad (13)$$

Sustituyendo las ecuaciones 11 y 12 en 13:

$$P_r = P_t \frac{\lambda^2 G_{TX} G_{RX}}{(4\pi r)^2} \quad (14)$$

III.2.2 Factor de normalización

La constante de normalización K_0 tiene que ser elegida de modo que la atenuación a la distancia $d_0 = 1$ m (la distancia de referencia para todos nuestros escenarios) y a la frecuencia de referencia f_c sea igual al valor PL_0 . Por lo tanto,

$$K_0 = \frac{P_r}{P_t} \frac{c^2}{4\pi f_c^2} \quad (15)$$

Donde c_0 es la velocidad de la luz en el espacio.

$$K_0 = \frac{(4\pi f_c^2)^2 P_0}{c^2} \quad (16)$$

III.2.3. Ganancia de Trayectoria

Finalmente, se muestra que la presencia de una persona (usuario) cerca de la antena atenúa la señal. Las mediciones muestran este proceso como estocástico, con variaciones en la atenuación entre 1dB y más de 10dB, dependiendo del usuario [Nelson *et al.*, 2001]. Sin embargo, para simplificar el modelo de este proceso, tiene que incluirse en todas los cálculos un “factor de atenuación de la antena”. Por lo tanto, la ganancia de trayectoria dependiente de la frecuencia está dada por (sustituyendo 14 y 16 en la ecuación 17):

$$G(f) = \frac{P_{rec}(f)}{P_{rad}(f)} = \frac{1}{4\pi R^2} \frac{P_{rec}(f)}{P_{rad}(f)} \frac{4\pi R^2}{\lambda^2} \frac{G_{eff}(f)}{G_{rad}(f)} \quad (17)$$

Nota: Los datos de eficiencia de la antena y la dependencia a la frecuencia los provee el vendedor.

III.2.4 Perfil de Retardo de Potencia (Power Delay Profile)

La respuesta a impulso del modelo SV (Saleh-Valenzuela) [Saleh & Valenzuela, 1987] está dada de manera general por

$$h(t) = \sum_{l=1}^L \sum_{k=1}^{K_l} a_{k,l} \exp(-j\phi_{k,l}) \delta(t - T_l - \tau_{k,l}) \quad (18)$$

donde ‘ $a_{k,l}$ ’ es el peso neto de la componente k_{th} en el cluster l_{th} , T_l es el retraso del l_{th} cluster, $\tau_{k,l}$ es el retraso del k_{th} componente multitrayectoria (MPC) relativo al tiempo de llegada T_l del l_{th} cluster. Las fases $\phi_{k,l}$ son variables aleatorias distribuidas

uniformemente en el rango $[0, 2\pi]$. El número de clusters L es un parámetro importante del modelo [Steinbauer & Molish, 2001]. Se asume que tiene una distribución de Poisson:

$$P(L) = \frac{e^{-\bar{L}} \bar{L}^L}{L!} \quad (19)$$

De manera que el número promedio de clusters \bar{L} caracteriza completamente la distribución.

La distribución de los tiempos de llegada de los clusters son dados por una distribución exponencial [Saleh & Valenzuela, 1987]

$$f(t) = \Lambda_1 e^{-\Lambda_1 t} \quad (20)$$

donde Λ_1 es el índice de llegada de clusters (se asumen independientes de l). El modelo SV clásico también usa un proceso de Poisson para la llegada de los rayos. Debido a la discrepancia entre medio interior de residencia y de oficina, se propone modelar la llegada de los rayos combinando dos procesos de Poisson, con la distribución para los tiempos de llegada dada por:

$$f(t) = \beta \lambda_1 e^{-\lambda_1 t} + (1 - \beta) \lambda_2 e^{-\lambda_2 t} \quad (21)$$

donde β es la probabilidad de la mezcla, y λ_1 y λ_2 son índices de llegada de los rayos.

III.2.5. Potencia de cluster y forma de cluster

El perfil de retardo de potencia (potencia media de las diferentes trayectorias) es exponencial en cada cluster

$$P_{\text{cluster}}(t) = \sum_l \Omega_l \exp(-\gamma_l t) \quad (22)$$

donde Ω_l es la energía integrada del l^{th} cluster, y γ_l es la constante del tiempo de retraso intra-cluster. Nótese que la normalización K_0 es aproximadamente uno, pero funciona para valores típicos de λ y γ .

Los índices de disminución de clusters generalmente dependen linealmente del tiempo de llegada del cluster,

$$\gamma_l \propto k_\gamma T_l + \gamma_0 \quad (23)$$

donde k_γ describe el incremento de la constante de disminución con retraso y γ_0 es el factor de decaimiento de los rayos.

La energía promedio (normalizada a γ_l), del l^{th} cluster sigue en general una caída exponencial

$$M_{\text{cluster}} = \sum_l \Omega_l \exp(-\gamma_l t) \quad (24)$$

donde M_{cluster} es una variable distribuida normalmente con desviación estándar σ_{cluster} .

Para el caso NLOS de algunos medios (oficina e industria), la forma del perfil de disminución de potencia puede ser distinto, a saber (en una escala log lineal)


(25)

Aquí, el parámetro χ describe la atenuación de la primera componente, el parámetro γ_{rise} determina que tan rápido incrementa a su máximo local el Perfil de Disminución de Potencia (PDP), y γ_1 determina la disminución en tiempos posteriores.

III.2.6 Desvanecimiento de Pequeña Escala

La distribución de las amplitudes de pequeña escala es Nakagami [Zhang, 2002]


(26)

donde $m \geq \frac{1}{2}$ es el factor m de Nakagami, $\Gamma(m)$ es la función gamma y Ω es el valor cuadrático medio de la amplitud. Es posible (aproximadamente) convertir a una distribución Rice con las ecuaciones de conversión:

$$m = \frac{K+1}{2} \quad (27)$$

y

$$K = \frac{\sqrt{m} m}{m \sqrt{m} m} \quad (28)$$

donde K y m son los factores Rice y Nakagami- m respectivamente.

El parámetro Ω corresponde a la potencia promedio y su dependencia al retraso está dada por el perfil de retraso de potencia recién definido. El parámetro m es modelado como

variable aleatoria distribuida lognormalmente cuyo logaritmo tiene una media μ_m y desviación estándar σ_m .

Ambos pueden depender del retraso

$$\mu_m = \hat{\mu}_m + \hat{\kappa}_m \tau \quad (29)$$

y

$$\sigma_m = \hat{\sigma}_m + \hat{\kappa}_\sigma \tau \quad (30)$$

Para el primer componente de cada cluster, el factor Nakagami se modela diferente. Se asume que es determinístico e independiente del retardo, donde $m = \tilde{m}_0$.

III.3. Parámetros y resultados

III.3.1 Parámetros

La sección previa consiste en las ecuaciones diseñadas para el modelo estadístico y utiliza los siguientes parámetros para obtener los resultados a varios fenómenos de canales de radio como respuesta a impulso, *excess delay*, *RMS delay* y perfil de decaimiento de potencia en este caso.

- PL_0 pérdida por trayectoria a una distancia de 1m
- n exponente de pérdida por trayectoria
- σ_s desviación estándar de sombreado
- A_{ant} pérdida por antena
- κ dependencia en frecuencia de la pérdida por trayectoria

- \bar{L} número promedio de clusters
- Λ índice de llegada inter-cluster
- $\lambda_1, \lambda_2, \beta$ índices de llegada de rayos (parámetros mezclados de modelo Poisson)
- Γ constante de decaimiento inter-cluster
- k_γ, γ_0 parámetros constantes de decaimiento intra-cluster
- $\sigma_{cluster}$ varianza de sombreado de cluster
- m_0, k_m , media del factor Nakagami m
- \hat{m}_0, \hat{k}_m , varianza del factor Nakagami m
- \tilde{m}_0 factor Nakagami m para componentes fuertes
- γ_{rise}, γ_1 y χ parámetros para forma PDP alternativa

III.3.2 Parámetros para LOS y NLOS

Hay dos conjuntos de resultados de Matlab para el modelo estadístico: LOS (line of sight) y NLOS (No-LOS). Los valores usados en los resultados de la simulación fueron

Tabla I: Valores de los parámetros usados para LOS y NLOS

	Interiores (LOS)
pérdida por trayectoria	
N	1.63
σ_s	1.9
PL_0	36.6
A_{ant}	3dB
K [dB/decade]	-3.5
Power delay profile	
\bar{L}	5.4
$\Lambda[1/ns]$	0.016
$\lambda_1, \lambda_2, \lambda_3 [1/ns]$	0.19, 2.97, 0.0184
$\Gamma[ns]$	14.6
k_γ	0
$\gamma_0[ns]$	6.4
$\sigma_{cluster}$ [dB]	NA
Small scale fading	
m_0	0.42dB
k_m	0
\hat{m}_0	0.31
\hat{k}_m	0
\tilde{m}_0	NA
χ	NA
γ_{rise}	NA
γ_1	NA

	Interiores (NLOS)
pérdida por trayectoria	
N	3.07
σ_s	3.9
PL_0	51.4
A_{ant}	3Db
K [dB/decade]	5.3
Power delay profile	
\bar{L}	1
$\Lambda[1/ns]$	NA
$\lambda_1, \lambda_2, \lambda_3 [1/ns]$	NA
$\Gamma[ns]$	NA
k_γ	NA
$\gamma_0[ns]$	NA
$\sigma_{cluster}$ [dB]	NA
Small scale fading	
m_0	0.50dB
k_m	0
\hat{m}_0	0.25
\hat{k}_m	0
\tilde{m}_0	
χ	0.86
γ_{rise}	15.21

III.3.3 Resultados de Matlab

1) LOS

Resultados para el escenario LOS dados, utilizando la respuesta al impulso, retardo en exceso, retardo rms y perfil de pérdida de potencia.

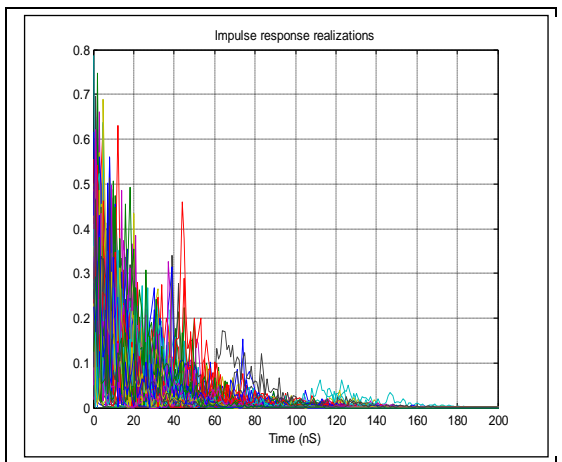


Figura 3: Respuesta a impulso (LOS)

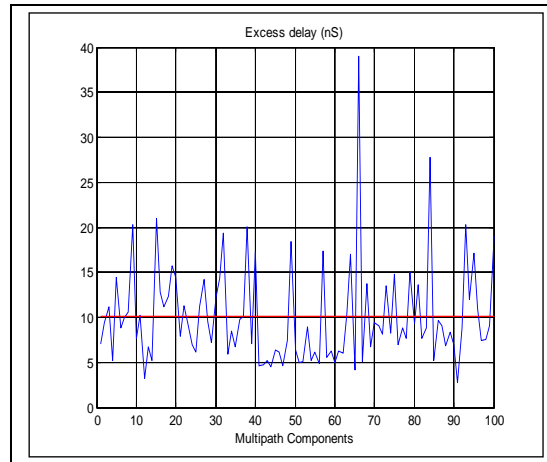


Figura 4: *Excess delay* (ns)

La figura 3 muestra la llegada de los clusters y rayos dentro del cluster, se nota que no llega ningún rayo después de los 200ns, que se relaciona con el esparcimiento máximo del retardo. La figura 4 muestra la variación del retardo de exceso para diferentes componentes multitrayectoria; se observa que el retardo de exceso promedio es de 10 ns. El pico observado en la componente multitrayectoria (MPC) = 65-66 se debe a multireflección de la señal.

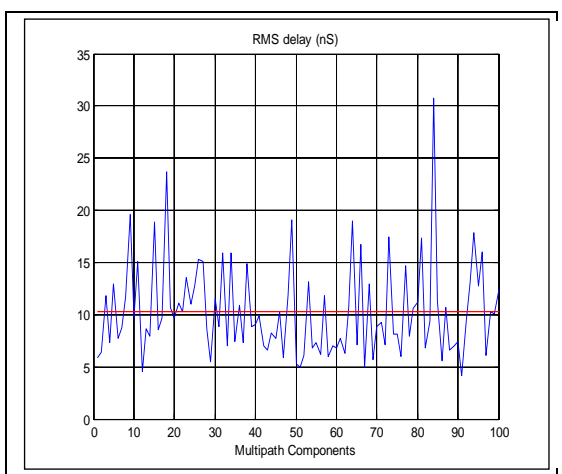


Figura 5: RMS delay (ns)

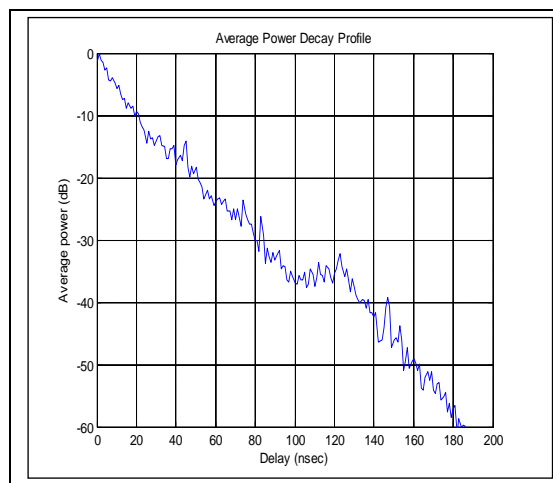


Figura 6: Perfil de pérdida de potencia

La figura 5 muestra la variación del retardo raíz-cuadrático medio (RMS) como función de la MPC. Se observa que el retraso de RMS promedio es de 10-11 ns. La figura 6 muestra el perfil de pérdida de potencia promedio como función del retardo. En la figura se considera 0 dBms como la máxima potencia recibida.

NLOS

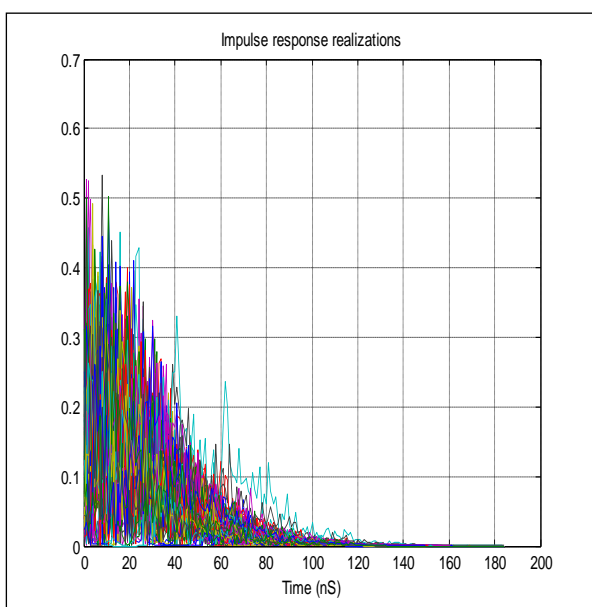


Figura 7: Respuesta a impulso (NLOS)

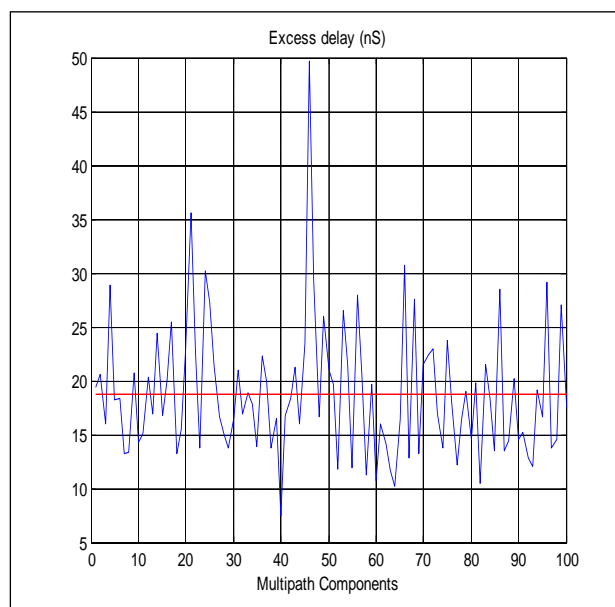


Figura 8: Retardo en exceso (ns)

Comparando la figura 7 con la respuesta a impulso en LOS se observa que las señales recibidas son más fuertes y duran más en LOS. Comparando la figura 8 con el escenario LOS se observa que en NLOS el retardo en exceso promedio aumenta a 19ns.

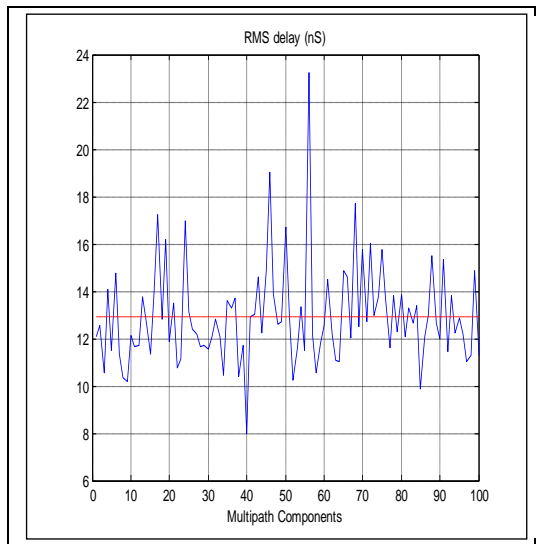


Figura 9: RMS delay (ns)

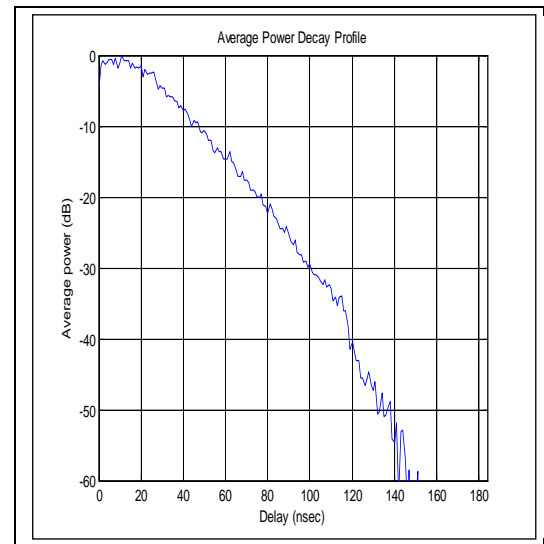


Figura 10: Perfil de pérdida de potencia

La figura 9 muestra la variación del retardo raíz cuadrático medio (*retardo RMS*) como función de MPC. Se observa que el promedio del retardo RMS es 13 ns, mayor que en el escenario LOS. La figura 10 muestra el perfil de pérdida de potencia promedio como función del retardo y comparando los escenarios LOS vemos que la pérdida de potencia se da más rápido en NLOS.

IV. Modelo determinístico para implementación en interiores

Este modelo ha sido diseñado específicamente para el segundo piso del edificio de la División de Física Aplicada del CICESE [Saúl, 2005] para red WIFI. Y fue modificado cambiando la frecuencia de operación a 2.4GHz, simulándola para recibir una potencia de hasta -90 dBms, cambiando el número de reflexiones y el lugar del transmisor y los receptores para poder usarlo con WSN. Estos cambios fueron necesarios porque con WSN la potencia de transmisión es bastante baja y eso hace que haya menos reflexiones de las

componentes multitrayectoria, además trabajan con una banda de frecuencia distinta y finalmente se simuló de acuerdo a la cobertura necesaria dependiendo de la sensibilidad de los receptores. El modelo se basa en una simulación con interface C++ y JAVA, para poder darle una presentación gráfica detallada a la cobertura del sensor o la combinación de sensores; también se muestra la distribución de potencia en el piso entero. El diseño en detalle y las modificaciones se explican en la tesis.

En esta sección, los resultados obtenidos de las mediciones físicas y el modelo determinístico modificado se comparan para la cobertura y el perfil de pérdida de potencia, probando la precisión del modelo determinístico para implementar WSN.

Cobertura: Cuando se comparan los resultados de la cobertura del modelo determinístico y las mediciones físicas se puede ver que es casi la misma para ambos.

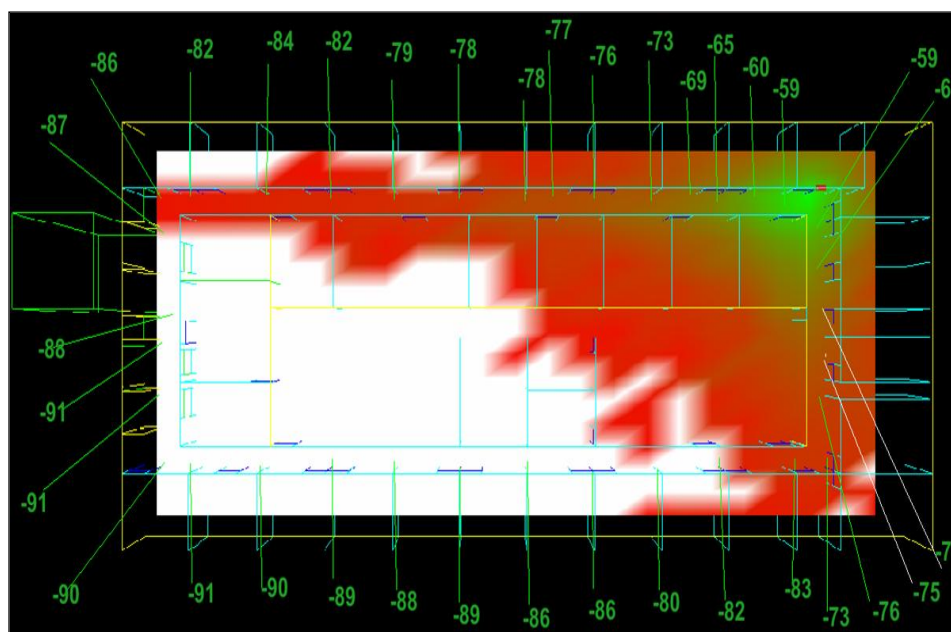


Figura 11: La cobertura para las lecturas medidas resulta hasta -87dBm , y el resultado de la cobertura del modelo determinístico es la de color en el fondo.

Pérdida de potencia: Comparando los resultados del modelo determinístico y las mediciones físicas, se observa que tienen un perfil de pérdida de potencia respecto a la distancia bastante similar, como se muestra en la figura 12.

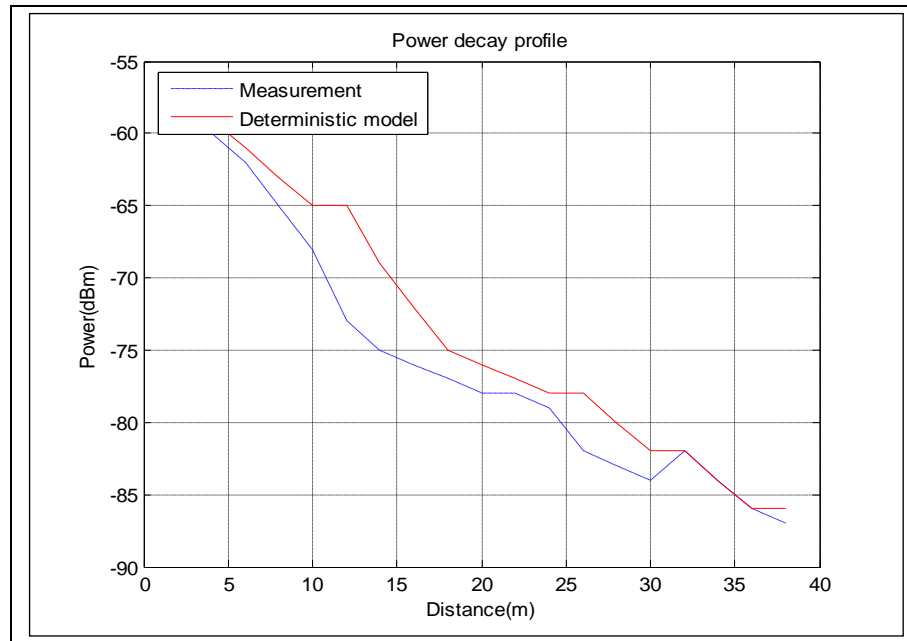


Figura 12: Comparación de pérdida de potencia

V. Conclusiones

Las conclusiones obtenidas de este trabajo son las siguientes:

- 1) El modelo estadístico diseñado (inspirado en el modelo Saleh Valenzuela) para WSN en interiores sirve para caracterizar el comportamiento del canal de radio y provee los parámetros básicos para caracterizar el canal, tales como pérdida de potencia, respuesta a impulso, esparcimiento del retardo y retardo RMS.

- 2) El modelo determinístico realmente ayuda a conocer la cobertura de los sensores colocados en cualquier parte del segundo piso del edificio de Física Aplicada del CICESE lo que puede ser beneficioso en la planeación de redes e implementación de algoritmos de enrutamiento. Con este modelo no solamente podemos saber la cobertura sino también la distribución de potencia en el piso entero. También nos da las mejores combinaciones de cobertura dependiendo del número de sensores que se quieran usar.
- 3) Las mediciones físicas tomadas para la cobertura del sensor en el piso son bastante similares a la información obtenida del modelo de canal de radio determinístico. Con el promedio de las series de mediciones se pudo observar que los resultados de cobertura obtenidos coinciden con los del modelo determinístico.
- 4) El canal radio en interiores es quasi-estático, varía con el tiempo **demasiado despacio** y sufre atenuaciones con el movimiento de personas. Durante las mediciones físicas se pudo observar que ante la presencia de obstáculos móviles había atenuación variable de señal.
- 5) Durante las mediciones se observó que la naturaleza y estadísticas de la respuesta al impulso del canal es virtualmente independiente del estado de polarización de las antenas transmisoras y receptoras (no válido fuera del campo visual).
- 6) El perfil de pérdida de potencia del modelo determinístico y las mediciones físicas son bastante similares y esto verifica la validez del modelo determinístico (Fig. 12).

- 7) El modelo estadístico se basa en una mezcla de dos procesos Poisson y se acopla de manera excelente con los tiempos de llegada de rayos comparando con el proceso de Poisson propuesto en el modelo S-V original.

CONTENTS

	Page
ABSTRACT.....	<i>ii</i>
ACKNOWLEDGMENTS.....	<i>v</i>
RESUMEN EJECUTIVO.....	<i>vii</i>
I. INTRODUCTION.....	
<i>I.1. Wireless Communication.....</i>	1
<i>I.2. Problem Description.....</i>	1
<i>I.3. Objective.....</i>	2
<i>I.4. Contribution of this thesis.....</i>	3
<i>I.5. Thesis Organization.....</i>	3
	4
II. RADIO CHANNEL AND REFERENCE MODEL.....	
<i>II.1. Introduction.....</i>	6
<i>II.2. Causes of radio irregularities.....</i>	6
II.2.1. Anisotropic path losses.....	6
II.2.2. Heterogeneous Sending Powers.....	7
<i>II.3. Types of radio channel Environment.....</i>	9
<i>II.4. Types of radio channel models.....</i>	10
II.4.1. Discrete channel models.....	12
II.4.2. Continuous channel models.....	12
II.4.3. Ray-tracing models.....	13
<i>II.5 Statistical Model and Deterministic Model.....</i>	13
II.5.1 Statistical Model.....	13
II.5.2 Deterministic Model.....	14
II.5.3 Combined statistical and deterministic modeling.....	15
<i>II.6 Reference Radio Channel Models.....</i>	15
II.6.1 Saleh and Valenzuela Model.....	16
II.6.2 Modified Saleh and Valenzuela Model.....	16
<i>II.6.2.1 Measurements.....</i>	20
<i>II.6.2.2 A Modified S-V clustering channel model.....</i>	20
	21
III. WIRELESS SENSOR NETWORK.....	
<i>III.1. Introduction.....</i>	23
<i>III.2. Networked wireless sensor devices.....</i>	23
<i>III.3. SKY T mote.....</i>	25
III.3.1. Key Features.....	27
III.3.2. Module description.....	28
III.3.3. Power.....	28
<i>III.4. IEEE 802.15.4 standard.....</i>	29
III.4.1. General description.....	30
III.4.2. How IEEE 802.15.4 is efficient for WSN?.....	30

CONTENT (continuation)

	Page
III.4.3. Approach used to make IEEE 802.15.4 low power and low cost....	32
III.5. The 2.4GHz band.....	33
IV. DESIGNED RADIO CHANNEL MODEL.....	34
<i>IV.1. Introduction.....</i>	<i>34</i>
<i>IV.2. Statistical model.....</i>	<i>34</i>
IV.2.1. Path loss.....	34
IV.2.2. Normalization factor.....	37
IV.2.3. Path gain.....	37
IV.2.4. Power decay profile.....	38
IV.2.5. Cluster power and cluster shape.....	39
IV.2.6. Auxillary parameters.....	41
IV.2.7. Small scale fading.....	44
IV.2.8. Generation of impulse response.....	45
<i>IV.3. Deterministic model.....</i>	<i>47</i>
IV.3.1. Designing of the model.....	48
V. MEASUREMENT AND RESULT ANALYSIS.....	54
<i>V.1. Introduction.....</i>	<i>54</i>
<i>V.2. Work done on Sky mote sensors.....</i>	<i>54</i>
V.2.1. Programming of motes.....	54
V.2.2. Java program.....	56
V.2.3. Power measurement.....	57
<i>V.3. Statistical model results.....</i>	<i>59</i>
V.3.1. Parameters.....	60
V.3.1. Line of sight (LOS).....	61
V.3.2. No line of sight (NLOS).....	66
<i>V.4. Deterministic model.....</i>	<i>71</i>
<i>V.5. Result analysis.....</i>	<i>72</i>
VI. CONCLUSIONS AND FUTURE WORK.....	75
<i>VI.1. Conclusions.....</i>	<i>75</i>
<i>VI.2. Future work.....</i>	<i>77</i>
<i>VI.3. Major contributions.....</i>	<i>78</i>
References.....	79

LIST OF FIGURES

Figure		Page
1	Signal Strength over Time in four directions	7
2	Signal Strength value in Different Directions	8
3	Radio irregularity with Sending Powers	9
4(a)	Exponentially decaying ray and cluster average powers	18
4(b)	Realization of Impulse response	18
5	Four spatially averaged power profiles within various rooms	19
6	Joint pdf for Cluster position under (a) LOS and (b) OLOS	22
7	Wireless Sensor Network	24
8	A Sky mote Sensor	29
9	Two different topology for IEEE 802.15.4 standard	31
10	Basic Structure of Second floor, Applied Physics, CICESE	48
11	Database for various materials with measurement	49
12	Grid Structure of the Second floor	50
13	Java interface for the Simulation	51
14	Java interface for addition of more sensors and changing location	51
15	Graphical representation of the Simulation result for coverage and Power profile	52
16	Network topology	55
17	Link quality indicator	55
18	ADC count display	56

LIST OF FIGURES (Continuation)

19	Java interface giving details for the different sensors connected in WSN and there respective sensor readings	57
20	Received Power (dBm) measurement on the second floor of Applied Physics building, CICESE	58
21	Received power (dBm) vs. distance (m)	59
22	Impulse response vs. time for LOS scenario	62
23	Excess delay with respect to Multipath components	63
24	RMS delay for Multipath components	64
25	Average power decay profile	65
26	Impulse response for the NLOS scenario vs. time	67
27	Excess delay for different Multipath components	68
28	RMS delay for Multipath components	69
29	Power decay profile for the NLOS scenario	70
30	Coverage and the power variation for second floor	71
31	Power decay vs. Distance	72
32	The coverage for the measured reading exits up to -87dBm, and the result of the coverage from deterministic model is on background in color.	73
33	Power decay comparison for Physical measurements and Deterministic Model output	74

LISTA DE FIGURAS

Figura		Página
1	Fuerza de la señal a través del tiempo en cuatro direcciones	7
2	Valor de la fuerza de la señal en diferentes direcciones	8
3	Irregularidad de radio con potencias enviadas	9
4(a)	Disminución exponencial de rayo y potencias promedio de cluster	18
4(b)	Realización de respuesta a impulso	18
5	Promedio de cuatro perfiles de potencia espaciados en varios cuartos	19
6	Pdf adjunto para posición de clusters bajo (a) LOS y (b) OLOS	22
7	Red de sensores inalámbricos (WSN)	24
8	Un sensor Sky tmote	29
9	Dos topologías distintas para estándar IEEE 802.15.4	31
10	Estructura básica del segundo piso, Física Aplicada, CICESE	48
11	Base de datos para varios materiales con medidas	49
12	Estructura de celdas para el segundo piso	50
13	Interface de Java para simulación	51
14	Interface Java para agregar más sensores y cambiar posiciones	51
15	Representación gráfica del resultado simulado de la cobertura y perfil de potencia	52
16	Topología de red	55
17	Indicador de calidad de enlace	55
18	Mostrador de cuenta ADC	56

LISTA DE FIGURAS (Continuación)

19	Interface Java dando detalles de los diferentes sensores conectados con WSN y sus lecturas respectivas	57
20	Mediciones de la potencia recibida (dBms) en el segundo piso del edificio de Física Aplicada, CICESE	58
21	Potencia recibida (dBms) vs. distancia (m)	59
22	Respuesta a impulso vs. Tiempo para escenario LOS	62
23	Retraso excesivo con respecto a componentes multitrayectoria	63
24	Retraso de RMS para componentes multitrayectoria	64
25	Perfil de pérdida de potencia promedio	65
26	Respuesta a impulso para escenario NLOS vs. tiempo	67
27	Retraso excesivo para diferentes componentes multitrayectoria	68
28	Retraso de RMS para componentes multitrayectoria	69
29	Perfil de pérdida de potencia para escenario NLOS	70
30	Cobertura y variación de potencia para el segundo piso	71
31	Pérdida de potencia vs. Distancia	72
32	La cobertura de las lecturas medidas llega hasta -87dBm, y el resultado de la cobertura con el modelo determinístico al fondo en color.	73
33	Comparación de pérdida de potencia para medidas físicas y resultados del modelo determinístico	74

LIST OF TABLES

Table		Page
I	Parameters used for LOS scenario	61
II	Parameters used for NLOS scenario	66

LISTA DE TABLAS

Tabla		Página
I	Parameters used for LOS scenario	61
II	Parameters used for NLOS scenario	66

Chapter I

Introduction

I.1 Wireless Communication

Wireless communications has the potential to provide the dream of the generation of communications services: access to any information anywhere and at any time. Wireless communications is the fastest and most exciting growth area in communications today, with new standards including WCDMA, CDMA-2000, WiFi, WiMAX, Bluetooth, ZigBee and many more appearing regularly, promising to revolutionize our lives with claims of true universal access.

The modern living and working environment is mostly an artificial environment, engineered over the past centuries. In order to better adapt this environment to human needs like health and safety as well as to reduce negative ecological effects, one needs to add smartness to the mechanisms that control and regulate environmental functions e.g. the flow of traffic or the air conditioning in office buildings. Today most of the technology in the form of algorithms and computation power are available; the missing link is a cheap, reliable and simple way to collect the needed data. Wireless sensor networks are a key technology with the promise to achieve these goals and will play an important role in many fields in the near future. The possible applications are numerous, ranging from environmental monitoring for smart buildings, maintenance, agriculture and meteorology to consumer applications and education.

Key features of a wireless sensor network are *ad-hoc networking* such that no manual network setup and maintenance is necessary, *ultra-low power consumption* to increase the lifetime of the entire network as well as *low cost* and *small size* to enable the ubiquitous use of hundreds of nodes in a network.

I.2 Problem Description

Wireless communications make use of electromagnetic waves to send signals through the air, covering long distances. From a user's perspective, wireless connections are not particularly different from any other network connection: your web browser, email, and other applications all work as you would expect. But radio waves have some unexpected properties compared to Ethernet cable. For example, it's very easy to see the path that an Ethernet cable takes: locate the plug sticking out of your computer, follow the cable to the other end and you find it. You can also be confident that running many Ethernet cables alongside each other won't cause problems, since the cables effectively keep their signals contained within the wire itself.

But how do you know where the waves emanating from your wireless card are going? What happens when these waves bounce off of objects in the room or other buildings in an outdoor link? How can several wireless cards be used in the same area without interfering with each other? In order to build stable wireless links, it is important to understand how radio waves behave in the real world. And, therefore is important to understand characteristics of the radio channel.

Therefore, in order to study the Wireless sensor network (WSN) there is need to understand the radio channel characteristics like impulse response of the channel, power decay in the channel, signal delay and hence there is need of a radio channel model which provides us with these parameters. As there is no existing radio channel model for wireless sensor network for indoor environment, there is requirement to design one for understanding the radio channel behavior for implementing wireless sensor network.

I.3 Objective

Main objective of this thesis is to design a radio channel model for wireless sensor network for indoor environment working in 2.4 GHz band.

The objective also includes the implementation of Sky motes which are based on IEEE 802.15.4 standard and analyze their coverage and power variations in real environment.

I.4 Contribution of this Thesis

As WSN (Wireless Sensor Network) is still a very new and developing field, there has been no reported work in field of radio channel model for WSN for indoor environment. The foremost and most important contribution of this thesis would be to propose the first Radio channel model for WSN for indoor environment. It is first designed radio channel model in the sense as the earlier model which is been used by various sensor making companies, just uses the pathloss between two sensors which is incomplete and does not provides with various other details of the radio channel. Whereas, this thesis proposes designed statistical radio channel model providing with basic radio channel behavior, like impulse response-

arrival of clusters and rays, excess delay, root mean square (RMS) delay and the power decay profile which in a great extent helps in achieving complete understanding about the channel behavior. The matlab simulation results have been presented in the thesis to support the objective.

This thesis has also used deterministic model specifically designed for the second floor of the applied physics building, based on the number of reflections, angle precision and power limit. This model provides with coverage from one sensor to combination of different sensors; it also gives a description for the power decay and hence could help in implementing efficient WSN. Designing of this model closely considers measurements for the entire floor and every structure along with permittivity and conductivity for different materials.

Finally physical reading for the coverage and power measurements between motes have been taken by programming them to transmit continuously and with the help of a 2.4GHz spectrum analyzer. Finally, the results of these three cases were compared in order to understand and conclude on the behavior of the radio channel for the indoor environment.

I.5 Thesis Organization

Chapter II presents the basics about the radio channel, causes of radio irregularities, different types of radio channel environments and different types of radio channel model.

This chapter also includes two reference models Saleh Valenzuela model and modified Saleh Valenzuela model.

Chapter III presents about wireless sensor network, properties of sensors, sky mote – the sensor used, IEEE 802.15.4 standard which is used by sensors and the 2.4GHz band.

Chapter IV presents the designed statistical radio channel model along with the complete mathematical model. It also includes the description of the deterministic model and various factors which are involved in the designing of the model.

Chapter V presents matlab simulation results for the designed statistical radio channel model and their explanation. It also presents the results of coverage and power decay profile for the deterministic model as well as the results of the physical measurements taken for mote coverage and received power profile. And finally the results are compared to reach a conclusion.

Chapter VI presents the final conclusions which are obtained from the results of statistical model and deterministic model; and other measurements. It also includes possible future work and contribution of this thesis.

Chapter II

Radio Channel and Reference Model

II.1 Introduction

Radio channel is an assigned band of frequencies sufficient for radio communication. The bandwidth of a radio channel depends upon the type of transmission and the frequency tolerance. A channel is usually assigned for a specified radio service to be provided by a specified transmitter. This chapter discusses about various causes of radio irregularities, different types of radio channel environment and different types of radio channel models. It also discusses the two important reference radio channel models that is Saleh Valenzuela model and modified Saleh Valenzuela model.

II.2 Cause of Radio Irregularities

Radio irregularity is caused by two types of factors: devices and the propagation media. Device properties include the antenna type (directional or omnidirectional), the sending power, antenna gains (at both the transmitter and receiver), receiver sensitivity, and the Signal to Noise-Ratio (SNR) threshold. Media properties include the media type, the background noise and some other environmental factors, such as the temperature and obstacles within the propagation media.

In general, the radio irregularity [Gang *et al.*, 2006] is caused by the anisotropic properties of the propagation media and the heterogeneous properties of devices. Among all these

factors, more focus is on the anisotropic path losses and the differences in signal sending power, which are commonly regarded as the key causes of radio irregularity.

II.2.1 Anisotropic Path Losses

The variance in the signal path loss is one of the major causes of radio irregularity. When a signal propagates within a medium, it may be reflected, diffracted, and scattered. Reflection occurs when an electromagnetic signal encounters an object, such as a wall, that is greater than the signal's wavelength. Diffraction occurs when the signal encounters an irregular surface, such as a stone with sharp edges. Scattering occurs when the medium through which the electromagnetic wave propagates contains a large number of objects smaller than the signal wavelength. The medium is normally different in different directions. Consequently, radio propagation exhibits anisotropic patterns in most environments.

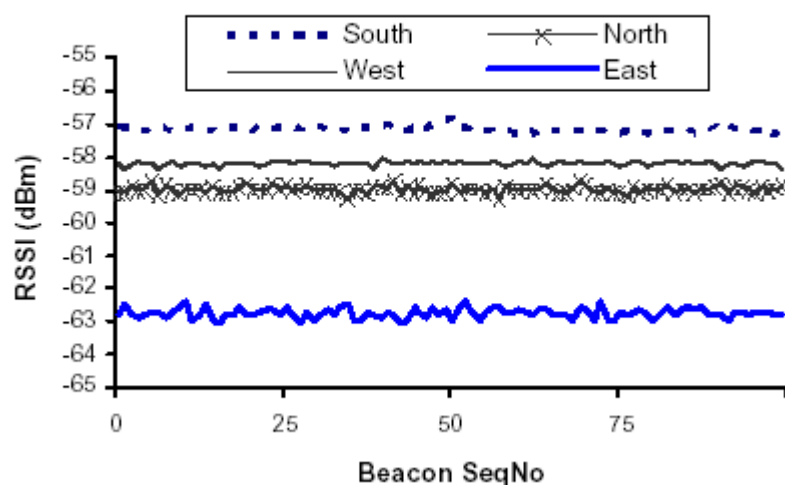


Figure 1: Signal Strength over Time in four directions.

Figura 1: Potencia de la señal a través del tiempo en cuatro direcciones.

Figure 1 [Gang *et al.*, 2006] shows that the received signal strength in each direction is relatively stable over time. However, the signal strength received in the south is much higher than that received in the east, although nodes have the same distance from the sender.

Figure 2 [Gang *et al.*, 2006] shows the variation of the received signal strength as a function of the angular direction with respect to the sender, when the distance between the sender and receiver is 10 feet and 20 feet, respectively. These results show that the received signal strength varies continuously with the direction. In other words, incremental changes in direction result in incremental variation in the received signal strength.

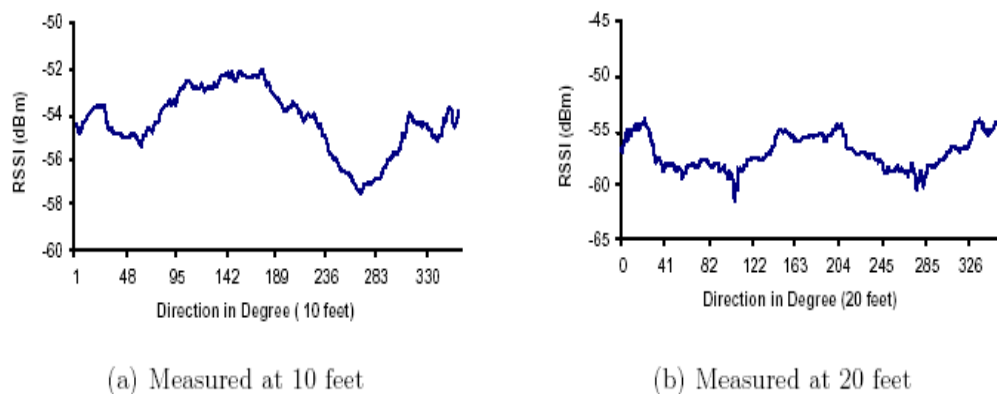


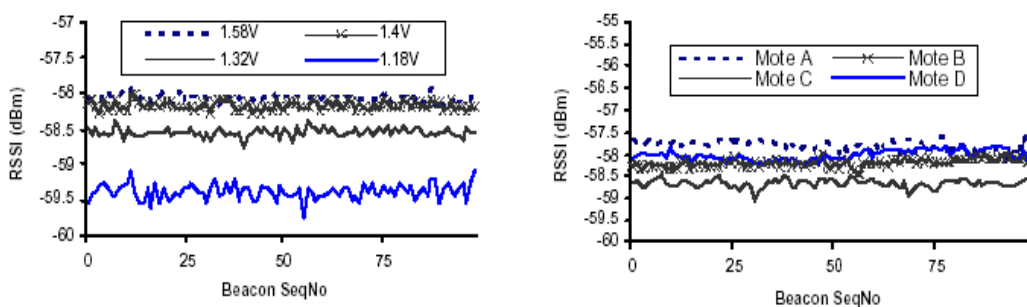
Figure 2: Signal Strength value in Different Directions.

Figura 2: Valor de la potencia de la señal en diferentes direcciones.

Another significant reason for anisotropic path loss is hardware differences. A node may not have the same antenna gain along all propagation directions, possibly due to hardware manufacturing. Hence, the anisotropic antenna gain of each node also contributes to the anisotropic path loss.

II.2.2 Heterogeneous Sending Powers

Sensor devices may transmit RF signal at different sending powers, even though they are the same kind of devices. This difference may arise from some random factors during the manufacture of sensor devices. In addition, after the sensor devices are deployed, the batteries of different sensor devices deplete at different rates, due to different workloads and different environments in which they are deployed. Heterogeneous sending powers result in variable communication ranges, and cause anisotropic connectivity [Gang *et al.*, 2006].



(a) One mote with different battery status (b) Different motes with the same battery status

Figure 3: Radio irregularity with Sending Powers.

Figura 3: Irregularidad de radio con potencias enviadas.

In Figure 3(a), the same sender and receiver is used, placed 10 feet apart. Each time the batteries at the sender side are changed. The result indicates that different battery status at the same sender can affect the received signal strength. In Figure 3(b), the same batteries are used, but in different senders each time. The same receiver is used, placed 10 feet apart from the sender. The result shows that different senders with the same batteries can also affect the received signal strength [Gang *et al.*, 2006].

II.3 Types of Radio Channel Environment

From the "call for applications", there are number of environments in which 802.15.4 devices should be operating. This list is not comprehensive, and cannot cover all possible future applications; however, it should be sufficient for the evaluation of the model:

1) Indoor residential: these environments are critical for "home networking", linking different appliances, as well as danger (fire, smoke) sensors over a relatively small area. The building structures of residential environments are characterized by small units, with indoor walls of reasonable thickness.

2) Indoor office: for office environments, some of the rooms are comparable in size to residential, but other rooms (especially cubicle areas, laboratories, etc.) are considerably larger. Areas with many small offices are typically linked by long corridors. Each of the offices typically contains furniture, bookshelves on the walls, etc., which adds to the attenuation given by the (typically thin) office partitioning.

3) Industrial environments: are characterized by larger enclosures (factory halls), filled with a large number of metallic reflectors. This is anticipated to lead to severe multipath.

4) Body-area network (BAN): communication between devices located on the body, e.g., for medical sensor communications, "wearable" cellphones, etc. Due to the fact that the main scatterers are in the near field of the antenna, and the generally short distances, the channel model can be anticipated to be quite different from the other environments.

5) Outdoor. While a large number of different outdoor scenarios exist, the current model covers only a suburban-like microcell scenario, with a rather small range.

6) Agricultural areas/farms: for those areas, few propagation obstacles (silos, animal pens), with large distances in between, are present. Delay spread can thus be anticipated to be smaller than in other environments

Remark: Other important environments are disaster areas, for the recovery of victims. Related important applications would include propagation through rubble (e.g., after an earthquake), again for victim recovery and communications between emergency personnel.

II.4 Types of Radio Channel Models

A variety of types of channel models are in use but here it considers only strict-sense channel models, i.e., channel models that include propagation effects but not interference. Advantages and disadvantages of the three major categories of channel models are presented in the following section but is more of a generic classification.

II.4.1 Discrete Channel Models

Note that the word “discrete” refers to the values of the model input and output, rather than time, which is discrete for both discrete and continuous channel models. Discrete channel models unite the modulator and demodulator, and possibly also forward error correction (FEC) coding, together with physical channel. Inputs to such a model are transition probabilities for symbols. These probabilities are in general time-varying and involve memory. Such models operate on sequences of bits or symbols, introducing errors to replicate the statistical behavior of the real demodulator output under stationary conditions.

The primary advantage of the discrete channel models is fast running times, i.e., computational requirement is minimal. On the other hand, with such a channel model it is impossible to separate the radio part of the model (hardware and signal processing algorithms used for modulation and demodulation) from the propagation channel part of the model, i.e., these two components of the physical layer become inextricably tangled. This is perhaps a good reason for excluding this category of channel model, since it is impossible to use them to make comparisons between different systems.

II.4.2 Continuous Channel Models

These models reproduce the effects of the channel propagation via a channel impulse response; in general, this impulse response must be time varying in order to account for both stochastic variation and changes in geometry (e.g., the distance from transmitter to receiver). With such models, a cleaner separation between the radio and channel models is possible; modulation and demodulation are no longer part of the channel model (antennas are still lumped with the channel). A given simulation must use a continuous channel model that has been sampled at the appropriate channel symbol rate; if values of the impulse response corresponding to a different time step are available, one can generally interpolate to produce values at the desired time step.

II.4.3 Ray-tracing Models

Computational requirements of ray-tracing models are such that they will not be integrated into network-level simulations in the near future. Ray-tracing models are, however, important because they hold out the hope for accurate off-line calculation of impulse responses for specified transmitter-receiver geometries, terrain types, and antennas. Once these impulse responses have been generated, they can be used in a moderately fast-running network model.

II.5 Statistical Model and Deterministic Model

Most commonly Radio channel models could be classified in following two important categories [Smulders *et al.*, 2002]:

- 1) Statistical Model
- 2) Deterministic Model

II.5.1 Statistical Model

Statistical models rely on measurement data and follow statistical impulse response modeling of the multipath fading channel first suggested by Turin. The goal of the statistical modeling is to investigate the distribution of the arrival time, amplitude and phase sequences, inter-relation between path variables, spatial correlations on path variables etc. In contrast site-specific propagation models are based on the use of electromagnetic wave propagation theory to characterize indoor radio propagation. This is a relatively new technique and has been proposed to predict path loss, the time invariant impulse response and the rms delay spread. It promises to provide fast and accurate prediction of indoor radio coverage and channel impulse response.

In statistical and empirical channel modeling, a number of channel characteristics are represented either directly or statistically from measurements of the radio channel. Empirical-statistical path loss models are often derived by applying linear regression on measured data. These models are chosen above their deterministic counterparts because of their simplicity and adequacy to calculate the average received signal power for grid areas as small as 50x50m. However, to achieve a higher accuracy in smaller areas (e.g. micro-cells), semi-empirical models are employed. These models are generally based on a theoretical model, which is then modified according to measured data for a particular propagation scenario.

II.5.2 Deterministic Model

Deterministic wave propagation models give the opportunity to obtain a physical insight in the actual propagation problem. They are appropriate in case when an accurate radio network planning is required, often as a benchmark. Depending on the modeling approach they can provide both narrow- and wideband analyses including delay-spread and angular-spread of the propagating waves. These results enable the design of modern wireless digital systems including smart antennas. In order to obtain deterministic propagation predictions for specific scenarios, topographical and material constants databases are required.

II.5.3 Combined statistical and deterministic modeling

Although currently available ray-tracing tools come in a wide variety with regard to the implementation of the ray-tracing algorithm itself, they are generally based on models of the same propagation mechanisms: line-of-sight propagation, reflection and diffraction. In a number of frequently occurring scenarios these mechanisms alone do not adequately explain the actually observed channel properties [Smulders *et al.*, 2002].

In the indoor scenarios, a complete description of the electromagnetic fields is hard to give, because very often the properties of the environment are not well defined or not always available. To improve the performance of existing ray-tracing tools for these scenarios new algorithms were recently developed these algorithms are based on a combination of statistical and deterministic modeling.

The output of the newly developed tools is an average value of the field strength or impulse response. In theory the corresponding variance can be made zero by a perfect description of the environment. In practice however, it is impossible to describe the environment in all its details.

II.6 Reference Radio Channel Models

For this thesis various radio channel models were referred, but the two most important models that have provided great guidance for this work are:

- 1) Saleh and Valenzuela Model
- 2) Modified Saleh and Valenzuela Model

II.6.1 Saleh and Valenzuela Model

Saleh and Valenzuela obtained their measurement results in medium-sized two story office buildings together with results from other researchers and developed a model for indoor radio channel simulation and analysis of various communication schemes. The model was shown to fit the measurements and may be extended to other buildings by adjusting its parameters [Saleh & Valenzuela, 1987]. The model assumes that:

1. Multipath components arrive in clusters.
2. The received amplitude of each component is an independent Raleigh random variable with a variance that decays exponentially with propagation delay, within a cluster.
3. The corresponding phase angles for each component are independent uniform random variables over $[0, 2\pi]$.

4. The clusters and multipath components within a cluster form a Poisson process with different rates.
5. The multipath components and the clusters have exponentially distributed inter-arrival times.
6. The formation of the clusters is related to building structure, while the multipath components within each cluster are formed by multiple reflections from objects in the vicinity of transmitter and receiver.

The model has enough flexibility to permit reasonably accurate fitting of the measured channel response and is simple enough for simulation. This model is successful for applications in office environment but its implementations in factory and other open environments are not that successful. The reason is that the environment in offices and in open buildings is inherently different and propagation is entirely dependent on environment.

There are 5 key parameters that define the S-V multipath channel model which are basic for designing radio channel model:

- 1) Λ is the cluster arrival rate
- 2) λ is the ray arrival rate, i.e. the arrival rate of path within each cluster
- 3) Γ is the cluster exponential decay factor
- 4) γ is the ray exponential decay factor
- 5) σ_a is the standard deviation of the lognormal fading term (dB).

Saleh-Valenzuela multipath model is given by the discrete time impulse response:

$$h_{discr}(t) = \sum_{l=0}^L \sum_{k=0}^K a_{k,l} \exp(j\phi_{k,l}) \delta(t - T_l - \tau_{k,l}) \quad (1)$$

Where:

L = number of clusters;

K_l = number of multipath components (MPC) or rays in the l_{th} cluster;

$\phi_{k,l}$ = phase of the k_{th} MPC in the l_{th} cluster

$\alpha_{k,l}$ = multipath gain coefficient of the k_{th} ray in the l_{th} cluster;

T_l = arrival time of the first ray of the l_{th} cluster;

$\tau_{k,l}$ = delay of the k_{th} ray within the l_{th} cluster relative to the first path arrival time

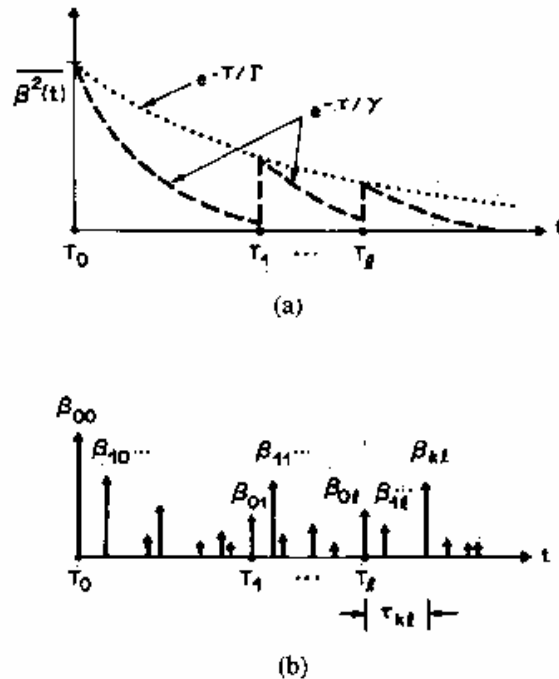


Figure 4: (a) Exponentially decaying ray and cluster average powers. (b) Realization of Impulse response.

Figura 4: (a) Disminución exponencial de rayo y potencias promedio de cluster. (b) Realización de respuesta al impulso

The figure 4(a) represents exponentially decaying of clusters average power as well as decaying of average power of rays in that cluster where $\overline{\beta^2}$ is the average power gain and the figure 4(b) illustrates the impulse response where $\beta_{k,l}$ is gain of the k_{th} ray of l_{th} cluster [Saleh & Valenzuela, 1987].

The clusters and rays form a Poisson arrival process with distributions given by:

$$P(T_l/T_{l-1}) = \Lambda \exp(-\Lambda(T_l - T_{l-1})), l > 0 \quad (2)$$

$$p(\tau_{k,l}/\tau_{(k-1),l}) = \lambda \exp(-\lambda(\tau_{k,l} - \tau_{(k-1),l})), k > 0 \quad (3)$$

Where: Λ = Cluster Arrival Rate; λ = Ray Arrival Rate.

Here it is assumed that all clusters have the same ray arrival rate, however, some measurements indicate that the arrival rate is larger for clusters that arrive later in time.

The multi-path gains are defined as follows:

$$\alpha_{k,l} = p_{k,l} \beta_{k,l} \quad (4)$$

With $p_{k,l}$ equiprobable ± 1 representing signal inversions due to reflections.

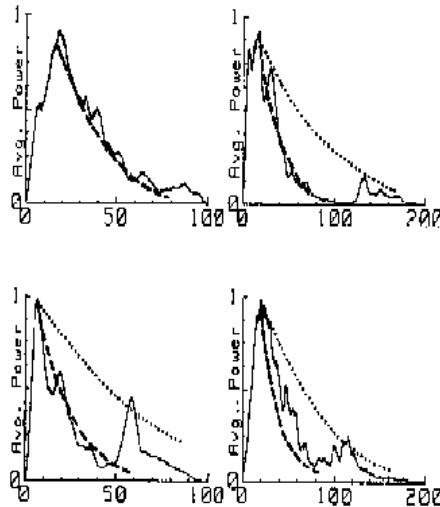


Figure 5: Four spatially averaged power profiles within various rooms.

Figura 5: Promedio espaciado de cuatro perfiles de potencia en varios cuartos.

Above figure 5 displays four spatially averaged power profiles within various rooms, the dashed lines correspond to exponential power decay profile of the rays and the clusters [Saleh & Valenzuela, 1987].

II.6.2 Modified Saleh Valenzuela Model

C. C. Chong et al. have proposed a new modified Saleh-Valenzuela (S-V) clustering channel model based on the measurement data collected in various types of high rise apartments under different propagation scenarios in the UWB (Ultra Wide Band) frequency band of 3-10 GHz. A new distribution, namely, a mixture of two Poisson processes, is proposed to model the ray arrival times. This new distribution fits the empirical data much better than the single Poisson process proposed in the conventional S-V model [Chong, *et al.*, 2003].

II.6.2.1 Measurements

Measurements were conducted using a network analyzer transmitting 1601 continuous waves tones uniformly distributed over the 3-10 GHz frequency range. This result in a frequency step of 4.375 MHz and gives a maximum excess delay of about 229.6 ns (i.e., a maximum distance of approximately 68.6 m). The 7 GHz bandwidth gives a temporal resolution of 142.9 ps and the sweeping time is adjusted to sweep across the bandwidth in 800 ms. Calibration was performed in an anechoic chamber with a 1 m reference distance to remove the antenna effects and was saved for post-processing. Measurements were conducted in various types of high-rise apartments with different sizes, layouts and

structures. In each apartment, the transmitter (TX) was fixed in the center of the living room, while the receiver (RX) was moved throughout the apartment around 8-10 different positions with TX/RX separation ranging from 1 to 20 m. It referred these different RX positions as local points. In order to characterize the small scale statistics of the channel, the RX was moved 25 times around each local point over a 55 square grid with 15 cm spacing between adjacent points. Each point on the grid is referred as a spatial point. Both line-of-sight (LOS) and no-LOS (NLOS) scenarios were considered. In order to confirm the time-invariant nature of the channel and for statistical analysis reliability, at each spatial point, 30 time-snapshots of the complex channel transfer functions (CTFs) were recorded.

II.6.2.2 A Modified S-V clustering channel model

Based upon the apparent existence of clusters in the measurement data, an UWB channel model which accounts for the clustering of multipath components (MPCs) was proposed; it was based on the conventional S-V channel model. The clustering Impulse response (CIR) can be expressed as follows:

$$h_{discr}(t) = \sum_{l=0}^L \sum_{k=0}^K a_{k,l} \exp(j\phi_{k,l}) \delta(t - T_l - \tau_{k,l}) \quad (5)$$

The proposed channel model relies on two classes of parameters, namely, intercluster and intra-cluster parameters, which characterize the cluster and Multipath Propagation Components (MPC), respectively. The distributions of the cluster arrival times, T_l and the ray arrival times, $\tau_{k,l}$ are given by two Poisson processes. According to the model, cluster inter-arrival times and ray intra-arrival times are described by the exponential *probability density functions* (PDFs) equations as mentioned above in original S.V. model with little

difference for ray arrival time. The measurement results show that the single Poisson process given in is insufficient to model the ray arrival times. Thus, proposes to model the ray arrival times with a mixture of two Poisson processes, so that

$$P(\tau_{k,l}/\tau_{(k-1),l}) \stackrel{\sim}{=} \beta \lambda_1 \exp \left[-\lambda_1(\tau_{k,l} - \tau_{(k-1),l}) \right] + (1 - \beta) \lambda_2 \exp \left[-\lambda_2(\tau_{k,l} - \tau_{(k-1),l}) \right], k > 0 \quad (6)$$

Where β is the mixture probability, while λ_1 and λ_2 are ray arrival rates.

In figure 6 some results from Modified S.V. Model have been demonstrated, as they represent joint pdf of cluster position for Line of Sight (LOS) and Obstructed-LOS (OLOS) [Chong, *et al.*, 2003].

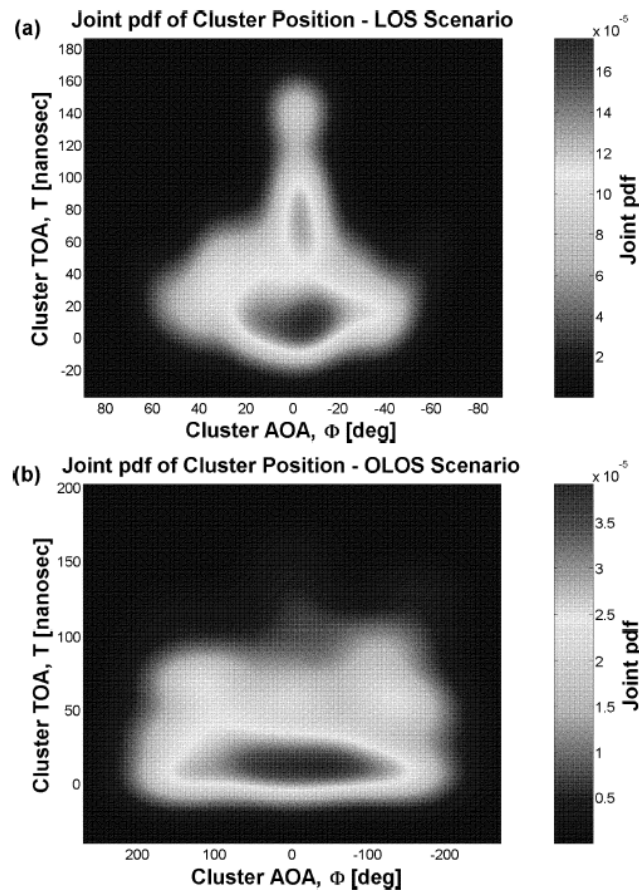


Figure 6: Joint pdf for Cluster position under (a) LOS and (b) OLOS.
 Figura 6: Pdf conjunta para posición de clusters por (a) LOS y (b) OLOS.

Chapter III

Wireless Sensor Network

III.1 Introduction

Municipalities worldwide are adopting Wireless Sensor Network (WSN) technology to make their cities safer, healthier, greener, and more productive, according to a recent research study by ON World.

The WSN solutions deployment for Smart Cities are being driven by increased spending on wireless broadband infrastructure, standards such as IEEE802.15.4 and ZigBee, increasing Green regulations, and the ongoing need for improved public safety.

Smart environments represent the next evolutionary development step in building, utilities, industrial, home, shipboard, and transportation systems automation. Like any sentient organism, the smart environment relies first and foremost on sensory data from the real world. Sensory data comes from multiple sensors of different modalities in distributed locations. The smart environment needs information about its surroundings as well as about its internal workings.

The challenges in the hierarchy of detecting the relevant quantities, monitoring and collecting the data, assessing and evaluating the information, formulating meaningful user displays, and performing decision-making and alarm functions are enormous. The

information needed by smart environments is provided by Distributed Wireless Sensor Networks, which are responsible for sensing as well as for the first stages of the processing hierarchy.

Figure 7 shows the complexity of wireless sensor networks, which generally consist of a data acquisition network and a data distribution network, monitored and controlled by a management center.

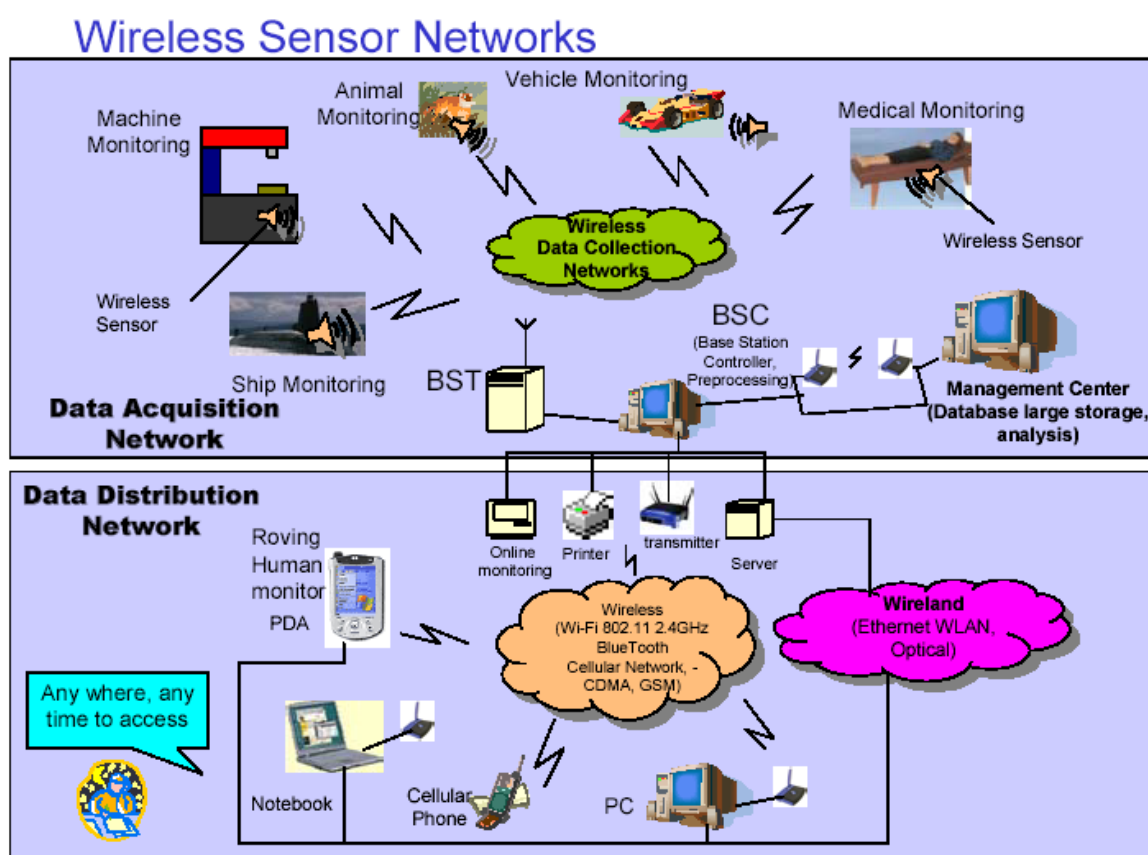


Figure 7: Wireless Sensor Network.

Figura 7: Red de sensores inalámbrica (WSN).

Sensor networks are the key to gathering the information needed by smart environments, whether in buildings, utilities, industrial, home, shipboard, transportation systems automation, or elsewhere. Recent terrorist and guerilla warfare countermeasures require distributed networks of sensors that can be deployed using, e.g. aircraft, and have self-organizing capabilities. In such applications, running wires or cabling is usually impractical. A sensor network is required that is fast and easy to install and maintain.

III.2 Networked wireless sensor devices

There are several key components that make up a typical wireless sensor network (WSN) device:

1. **Low-power embedded processor:** The computational tasks on a WSN device include the processing of both locally sensed information as well as information communicated by other sensors. At present, primarily due to economic constraints, the embedded processors are often significantly constrained in terms of computational power (e.g., many of the devices used currently in research and development have only an eight-bit 16-MHz processor).

Due to the constraints of such processors, devices typically run specialized component-based embedded operating systems, such as Tiny OS.

2. **Memory/storage:** Storage in the form of random access and read-only memory includes both program memory (from which instructions are executed by the processor), and data

memory (for storing raw and processed sensor measurements and other local information). The quantities of memory and storage on board a WSN device are often limited primarily by economic considerations but also in order to maintain small size of a sensor.

3. **Radio transceiver:** WSN devices include a low-rate, short-range wireless radio (10–100 kbps, <100 m). While currently quite limited in capability too, these radios are likely to improve in sophistication over time – including improvements in cost, spectral efficiency, tunability, and immunity to noise, fading, and interference. Radio communication is often the most power intensive operation in a WSN device, and hence the radio must incorporate energy-efficient sleep and wake-up modes.

4. **Sensors:** Due to bandwidth and power constraints, WSN devices primarily support only low-data-rate sensing. Many applications call for multi-modal sensing, so each device may have several sensors on board. The specific sensors used are highly dependent on the application; for example, they may include temperature sensors, light sensors, humidity sensors, pressure sensors, accelerometers, magnetometers, chemical sensors, acoustic sensors, or even low-resolution imagers.

5. **Geopositioning system:** In many WSN applications, it is important for all sensor measurements to be location stamped. The simplest way to obtain positioning is to pre-configure sensor locations at deployment, but this may only be feasible in limited deployments. Particularly for outdoor operations, when the network is deployed in an *ad hoc* manner, such information is most easily obtained via satellite-based GPS.

6. **Power source:** For flexible deployment the WSN device is likely to be battery powered (e.g. using LiMH AA batteries). While some of the nodes may be wired to a continuous power source in some applications, and energy harvesting techniques may provide a degree of energy renewal in some cases, the finite battery energy is likely to be the most critical resource bottleneck in most WSN applications. Depending on the application, WSN devices can be networked together in a number of ways. In basic data-gathering applications, for instance, there is a node referred to as the *sink* to which all data from *source* sensor nodes are directed. The simplest logical topology for communication of gathered data is a single-hop star topology, where all nodes send their data directly to the sink

III.3 SKY Tmote

Sky Tmote [Tmote, 2007] is an ultra low power wireless module for use in sensor networks, monitoring applications, and rapid application prototyping. Tmote Sky leverages industry standards like USB and IEEE 802.15.4 to interoperate seamlessly with other devices. By using industry standards, integrating humidity, temperature, and light sensors, and providing flexible interconnection with peripherals, Tmote Sky enables a wide range of mesh network applications. Tmote Sky is a drop-in replacement for Moteiv's successful Telos design. Tmote Sky includes increased performance, functionality, and expansion. With TinyOS support out-of-the-box, Tmote Sky leverages emerging wireless protocols and the open source software movement. Tmote Sky is part of a line of modules featuring on-board sensors to increase robustness while decreasing cost and package size.

III.3.1 Key Features

In this section it presents the important characteristics of the Sky tmote which are used in this work for all experiment purposes [Tmote, 2007].

- 1) 250kbps 2.4GHz IEEE 802.15.4 Chipcon Wireless Transceiver
- 2) Interoperability with other IEEE 802.15.4 devices
- 3) 8MHz Texas Instruments MSP430 microcontroller (10k RAM, 48k Flash)
- 4) Integrated ADC, DAC, Supply Voltage Supervisor, and DMA Controller
- 5) Integrated onboard antenna with 50m range indoors / 125m range outdoors
- 6) Integrated Humidity, Temperature, and Light sensors
- 7) Ultra low current consumption
- 8) Fast wakeup from sleep ($<6\mu\text{s}$)
- 9) Hardware link-layer encryption and authentication
- 10) Programming and data collection via USB
- 11) 16-pin expansion support and optional SMA antenna connector
- 12) TinyOS support: mesh networking and communication implementation
- 13) Complies with FCC Part 15 and Industry Canada regulations
- 14) Environmentally friendly – complies with RoHS (the restriction of the use of certain hazardous substances in electrical and electronic equipment) regulations

III.3.2 Module Description

The Tmote Sky module is a low power “mote” with integrated sensors, radio, antenna,

Microcontroller and programming capabilities. The figure 8 shows how a Sky tmote physically looks like.



Figure 8: A Sky Tmote Sensor.

Figura 8: Un sensor Sky Tmote.

III.3.3 Power

Tmote Sky may be powered by two AA batteries. The module was designed to fit the two AA battery form factor. AA cells may be used in the operating range of 2.1 to 3.6V DC; however the voltage must be at least 2.7V when programming the microcontroller flash memory or external flash memory. If the Tmote Sky module is plugged into the USB port for programming or communication, it will receive power from the host computer. The mote operating voltage when attached to Universal serial bus (USB) is 3V. If Tmote will always be attached to a USB port, no battery pack is necessary.

III.4 IEEE 802.15.4 standard

III.4.1 General Description

A Low Range – Wide Personal Area Network (LR-WPAN) is a simple, low-cost communication network that allows wireless connectivity in applications with limited power and relaxed throughput requirements. The main objectives of an LR-WPAN are ease of installation, reliable data transfer, short-range operation, extremely low cost, and a reasonable battery life, while maintaining a simple and flexible protocol [IEEE Std., 2004].

Some of the characteristics of an LR-WPAN are

- 1) Over-the-air data rates of 250 kb/s, 40 kb/s, and 20 kb/s
- 2) Star or peer-to-peer operation
- 3) Allocated 16 bit short or 64 bit extended addresses
- 3) Allocation of guaranteed time slots (GTSs)
- 4) Carrier sense multiple access with collision avoidance (CSMA-CA) channel access
- 5) Fully acknowledged protocol for transfer reliability
- 6) Low power consumption
- 7) Energy detection (ED)
- 8) Link quality indication (LQI)
- 9) 16 channels in the 2450 MHz band, 10 channels in the 915 MHz band, and 1 channel in the 868 MHz band

Two different device types can participate in an LR-WPAN network; a full-function device (FFD) and a reduced-function device (RFD), as can also be seen in figure 9. The FFD can operate in three modes serving as a personal area network (PAN) coordinator, a

coordinator, or a device. An FFD can talk to RFDs or other FFDs, while an RFD can talk only to an FFD. An RFD is intended for applications that are extremely simple, such as a light switch or a passive infrared sensor; they do not have the need to send large amounts of data and may only associate with a single FFD at a time. Consequently, the RFD can be implemented using minimal resources and memory capacity.

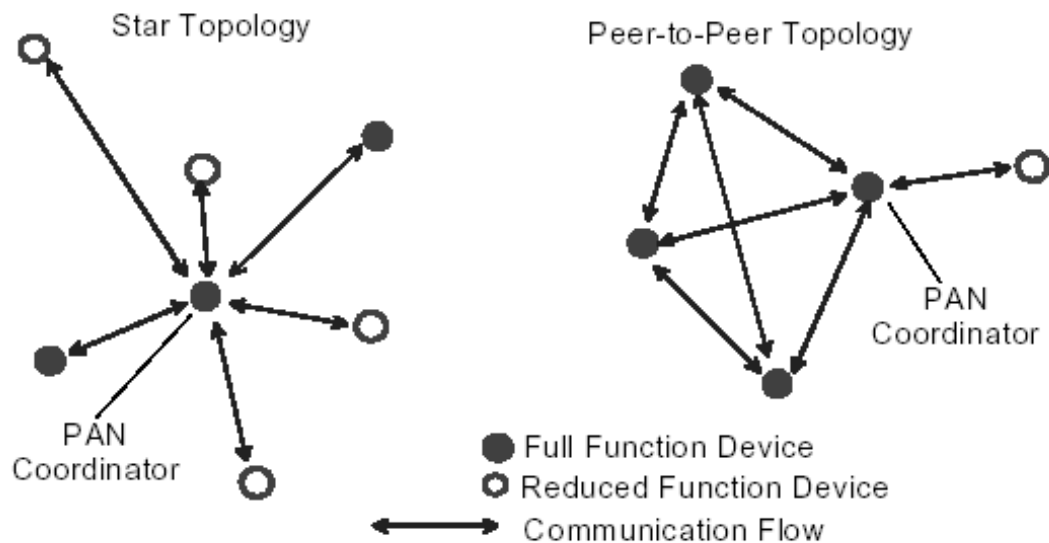


Figure 9: Two different topologies for IEEE 802.15.4 standard.

Figura 9: Dos topologías distintas para el estándar IEEE 802.15.4.

A well-defined coverage area does not exist for wireless media because propagation characteristics are dynamic and uncertain. Small changes in position or direction may result in drastic differences in the signal strength or quality of the communication link. These effects occur whether a device is stationary or mobile as moving objects may impact station-to-station propagation [IEEE Std., 2004].

III.4.2 How IEEE 802.15.4 is efficient for WSN?

This section specifies various features of IEEE 802.15.4 standard that makes it efficient for WSN.

- 1) Use of long beacon periods and the battery life extension mode.
- 2) The active period of a beaconing node can be reduced, allowing the node to sleep between beacons.
- 3) Network node in control of the network (PAN coordinator) scans other available channels to find a more suitable channel measuring the peak energy present in each alternative channel and then uses this information to select a suitable channel.
- 4) A link quality indication (LQI) byte is attached to each received frame by the physical layer

III.4.3 Approach used to make IEEE 802.15.4 low power and low cost

In order to achieve the low power and low cost goals established by IEEE 802.15.4 and to inform design trade-off decisions, the following approaches are taken:

- 1) Reduce the amount of data transmitted
- 2) Reduce the transceiver duty cycle and frequency of data transmissions
- 3) Reduce the frame overhead
- 4) Reduce complexity
- 5) Reduce range
- 6) Implement strict power management mechanisms (power-down and sleep modes)

III.5 The 2.4 GHz Band

The 2400 – 2483.5 MHz frequency band, hereafter referred to as “the 2.4 GHz band”, is being used for an increasingly diverse range of applications. These include: Electronic News Gathering / Outside Broadcast; radio frequency identification devices; lighting; microwave ovens; public telecommunications; short range radio devices and low power audio, video and data links (including RLAN, Bluetooth, HomeRF). This diverse, and increasingly intensive, use of the band brings with it the potential for congestion and consequent possible degradation in service quality.

Historically, the 2.4 GHz band has been license exempt for private users, although it has been regulated with regard to power levels that may be used. It is therefore an inherently anarchic environment, with unpredictable levels of interference leading to potentially erratic levels of service quality.

Arguably, such an environment may seem inappropriate for safety critical and public services where an agreed quality of service must be guaranteed. However, the band has a number of attractions. In first place, its relatively low frequency makes it appropriate for mobile / nomadic communications. Secondly, its global availability offers a rare opportunity for manufacturers to take advantage of the economies of scale that come with operations in a world wide market.

Chapter IV

DESIGNED RADIO CHANNEL MODEL

IV.1 Introduction

This chapter discusses about designed statistical radio channel model for Wireless Sensor network, for indoor environment. It presents the mathematical analysis, equations that helped in the designing of the statistical radio channel model. Here the designing of the deterministic model is also discussed [Saul, 2005], specifically designed for the second floor of Applied Physics building, CICESE. This model was modified and used for WSN in this thesis, to verify few results of the designed statistical model, as there is no other radio channel model for WSN (indoor environment) for comparing the results.

IV.2 Statistical Model

This designed model is influenced by modified Saleh Valenzuela work, defining the various important radio channel characteristics in order to understand the radio channel behavior in case of LOS (Line of sight) and NLOS (No-LOS). It mentions the entire process step by step as following.

IV.2.1 Path loss

The computation of the received power should proceed the following way:

1) In a first step, it has to be defined the transmit power spectrum $P_t(f)$ that will be seen "on air".

This spectrum is the product of the output spectrum of the transmit amplifier $P_{TX-amp}(f)$, i.e., as seen at the antenna connector with the frequency dependent antenna efficiency $\eta_{TX-ant}(f)$.

$$P_t(f) = P_{TX-amp}(f) \cdot \eta_{TX-ant}(f) \quad (7)$$

From [Kadel & Lorenz, 1995] and [Rossi, 1999] pathloss could be better described as a function of frequency as well as distance according to equation 8.

$$PL(f, d) \propto PL(f) \cdot PL(d) \quad (8)$$

The frequency dependence of the pathloss is given as [Qui & Lu, 1996]

$$\sqrt{PL(f)} \propto f^{-k} \quad (9)$$

Where k is frequency dependence of the pathloss and the distance dependence of the pathloss in dB is described by

$$PL(d) = PL_0 + 10n \log_{10} \left(\frac{d}{d_0} \right) \quad (10)$$

where reference distance (d_0) is set to 1m and PL_0 is the pathloss at the reference distance.

n is the pathloss exponent which depends on the environment, for LOS in indoor environment it is 1 in corridor to about 2 in office environment and for NLOS it ranges from 3 to 4 [U.C.A.N., 2003].

2) In the next step using equations 8, 9 and 10, we compute the frequency-dependent power density at a distance d ,

$$\hat{P}(f, d) = K_0 \frac{P_t(f)}{4\pi d_0^2} \left(\frac{d}{d_0} \right)^{-n} \left(\frac{f}{f_c} \right)^{-2k} \quad (11)$$

Where f_c is a reference frequency; the normalization constant K_0 will be determined later on, and $n = 2$.

3) Finally, the received frequency-dependent power $P_r(d, f)$ has to be determined, by multiplying the power density $\hat{P}(f, d)$ at the location of the receiver with the antenna effective area A_{RX}

$$A_{RX}(f) = \frac{\lambda^2}{4\pi} G_{RX}(f) \quad (12)$$

where G_{RX} is the receive antenna gain; and also multiply with the antenna efficiency $\eta_{RX-ant}(f)$. Since we are again assuming that the radiation is averaged over all incident angles, the antenna gain is unity, independent of the considered frequency. The frequency-dependent received power is then given by

$$P_r(f, d) = \hat{P}(f, d) \cdot A_{RX}(f) \cdot \eta_{RX-ant}(f) \quad (13)$$

Substituting equation 11 and 12 in equation 13:

$$P_r(d, f) = K_0 P_{TX-amp}(f) \eta_{TX-ant}(f) \eta_{RX-ant}(f) \frac{c_0^2}{(4\pi d_0 f_c)^2} \frac{1}{\left(\frac{d}{d_0}\right)^2 \left(\frac{f}{f_c}\right)^{2k+2}} \quad (14)$$

IV.2.2 Normalization Factor

The normalization constant K_0 has to be chosen in such a way that the attenuation at distance $d_0 = 1$ m (the reference distance for all of our scenarios), and at the reference frequency f_c is equal to a value PL_0 . Thus,

$$\frac{P_r(d_0, f_c)}{P_{TX-amp}(f_c)} = PL_0 = K_0 \frac{c_0^2}{(4\pi d_0 f_c)^2} \quad (15)$$

Where c_0 is speed of light in free space.

$$K_0 = \frac{(4\pi d_0 f_c)^2}{c_0^2} PL_0 \quad (16)$$

IV.2.3. Path Gain

Finally, it has been shown that the presence of a person (user) close to the antenna will lead to attenuation. Measurements have shown this process to be stochastic, with attenuations varying between 1dB and more than 10dB, depending on the user [Nelson *et al.*, 2001]. However, for the sake of simplicity to model this process, an "antenna attenuation factor" has to be included in all computations. Therefore the frequency-dependent path gain will be given by (substituting 14 and 16 in the equation 17):

$$PG(d, f) = \frac{P_r(d, f)}{P_{TX-amp}(f)} = \frac{1}{2} PL_0 \eta_{TX-ant}(f) \eta_{RX-ant}(f) \frac{\left(\frac{f}{f_c}\right)^{-2(k+1)}}{\left(\frac{d}{d_0}\right)^n} \quad (17)$$

Note: The Antenna efficiency and its frequency dependence are to be provided by vendor.

IV.2.4 Power Delay Profile

The impulse response of the SV (Saleh-Valenzuela) [Saleh & Valenzuela, 1987] model is given in general as

$$h_{discr}(t) = \sum_{l=0}^L \sum_{k=0}^K a_{k,l} \exp(j\phi_{k,l}) \delta(t - T_l - \tau_{k,l}) \quad (18)$$

where ‘ $a_{k,l}$ ’ is the tap weight of the k_{th} component in the l_{th} cluster, T_l is the delay of the l_{th} cluster, $\tau_{k,l}$ is the delay of the k_{th} MPC relative to the l_{th} cluster arrival time T_l . The phases $\phi_{k,l}$ are uniformly distributed, that is uniformly distributed random variable from the range $[0, 2\pi]$. The number of clusters L is an important parameter of the model [Steinbauer & Molish, 2001]. It is assumed to be Poisson-distributed

$$pdf_L(L) = \frac{(\bar{L})^L \exp(-\bar{L})}{L!} \quad (19)$$

so that the mean \bar{L} completely characterizes the distribution.

The distributions of the cluster arrival times are given by a Poisson process [Saleh & Valenzuela, 1987]

$$p(T_l/T_{l-1}) = \Lambda_l \exp \left[-\Lambda_l (T_l - T_{l-1}) \right], l > 0 \quad (20)$$

where Λ_l is the cluster arrival rate (assumed to be independent of l). The classical SV model also uses a Poisson process for the ray arrival times. Due to the discrepancy in the fitting for the indoor residential and indoor office environment, propose to model ray arrival times with mixtures of two Poisson processes as follows:

$$p(\tau_{k,l}/\tau_{(k-1),l}) = \beta \lambda_1 \exp \left[-\lambda_1 (\tau_{k,l} - \tau_{(k-1),l}) \right] + (1 - \beta) \lambda_2 \exp \left[-\lambda_2 (\tau_{k,l} - \tau_{(k-1),l}) \right], k > 0 \quad (21)$$

where β is the mixture probability, while λ_1 and λ_2 are ray arrival rates.

IV.2.5 Cluster power and cluster shape

The power delay profile (mean power of the different paths) is exponential within each cluster:

$$E |a_{k,l}|^2 = \Omega_l \frac{1}{\gamma_l \left[(1 - \beta) \lambda_1 + \beta \lambda_2 + 1 \right]} \exp(-\tau_{k,l} / \gamma_l) \quad (22)$$

where Ω_l is the integrated energy of the l th cluster, and γ_l is the intra-cluster decay time constant. Note that the normalization K_0 is approximately one, but works for typical values of λ and γ .

The cluster decay rates are found to depend linearly on the arrival time of the cluster,

$$\gamma_l \propto k_\gamma T_l + \gamma_0 \quad (23)$$

Where k_γ describes the increase of the decay constant with delay and γ_0 is ray decay factor. Considering the case of indoor office environment, there are not many multiple reflections of signals and hence there are not that many arriving clusters; therefore for indoor office environment the value of k_γ remains zero for LOS and for NLOS case it is definitely not applicable. But had it been a scenario where there is multiple reflection of the signal, like one of indoor industrial environment, k_γ would definitely have a value for LOS case.

The mean energy (normalized to γ_l), of the l th cluster follows in general an exponential decay:

$$10 \log \Omega_l \stackrel{d}{=} 10 \log \left(\exp \left(\frac{-T_l}{\Gamma} \right) \right) + M_{cluster} \quad (24)$$

where $M_{cluster}$ is a normally distributed variable with standard deviation $\sigma_{cluster}$.

For the NLOS case of some environments (office and industrial), the shape of the power delay profile can be different, namely (on a log-linear scale)

$$E \left[|a_{k,l}|^2 \right] \stackrel{d}{=} \left(1 - \chi \cdot \exp \left(\frac{-\tau_{k,l}}{\gamma_{rise}} \right) \right) \cdot \exp \left(\frac{-\tau_{k,l}}{\gamma_1} \right) \cdot \frac{\gamma_1 + \gamma_{rise}}{\gamma_1} \cdot \frac{\Omega_1}{\gamma_1 + \gamma_{rise} (1 - \chi)} \quad (25)$$

Here, the parameter χ describes the attenuation of the first component, the parameter γ_{rise} determines how fast the Power Decay Profile (PDP) increases to its local maximum, and γ_1 determines the decay at late times.

IV.2.6 Auxiliary parameters

Parameters that are helpful in many contexts are the mean excess delay, rms delay spread, and the number of multipath components that are within 10 dB of the peak amplitude.

Measuring Delay Spread: Mean delay and delay spread are tied to the uncorrelated scattering assumption. In this case, the correlation matrix of the channel is diagonal, and can be obtained by averaging several measured impulse responses, also referred to as the power delay profile. The mean delay is now the mean of the PDP, the delay spread is the standard deviation of the PDP. Thus both parameters together are a measure about the number of independently fading taps and thus about the diversity order, although not in a precise way as analyzed above. For these numbers to be meaningful, the PDP needs to be compactly supported and also otherwise mathematically well behaved, an assumption which can almost always be made for the channels under consideration.

The excess delay can be simply defined as the first moment of the PDP as shown in following equation [Tadeuz & Zepernick, 2000]

$$\bar{\tau} = \frac{\sum_l P_l \tau_l}{\sum_l P_l} \quad (26)$$

The rms delay spread can be defined as the second central moment of the PDP [Tadeuz & Zepernick, 2000]:

$$\sigma_\tau = \sqrt{\tau^2 - (\bar{\tau})^2} \quad (27)$$

Measurement of clustering parameters:

This section presents measurements of five key parameters in clustering effects, which are:

- 1) Λ , the cluster arrival rate
- 2) λ , the ray arrival rate, i.e. the arrival rate of path within each cluster
- 3) Γ , the cluster exponential decay factor
- 4) γ , the ray exponential decay factor
- 5) σ_a , the standard deviation of the lognormal fading term (dB).

The main characteristics of the channel that are used to derive above model parameters are the following:

- 1) Mean excess delay
- 2) rms delay spread

From [Spencer *et al.*, 2000], the cluster and ray decay time constants, Γ and γ , were first estimated by superimposing clusters with normalized amplitudes and time delays, then selecting a mean decay rate. For example, in order to estimate Γ , the first cluster arrival in each set was normalized to amplitude of one and a time delay of zero. All cluster arrivals were superimposed and plotted on a semi-logarithmic plot. The estimate for Γ was found by curve fitting the line (representing an exponential curve) such that the mean squared error was minimized. Similarly, in order to estimate γ , the first arrival in each cluster was set to a time of zero and amplitude of one, and all other ray arrivals were then adjusted accordingly and superimposed. Following this model, the best fit exponential distributions were determined from the cluster and ray arrival times, respectively. In order to estimate the Poisson cluster arrival rate, Λ the first arrival in each cluster was considered to be the beginning of the cluster, regardless of whether or not it had the largest amplitude. The arrival time of each cluster was subtracted from its successor, so that the conditional probability distribution given in equation 20 could be estimated. The Poisson ray arrival rate, λ was guessed based on the average separation time between arrivals. The estimates for Λ and λ were both obtained by fitting the sample *pdf* to the corresponding probability for each bin. The fitting was done using a least mean square criterion.

For the case of overlapping clusters, a procedure as proposed in [Erceg *et al.*, 2003] is referred. By assuming that each cluster has an exponential shape, a straight-line extrapolation function (in dB) is deployed on the first cluster and then subtracts the PDP of the first cluster from the total PDP. Then, the next non-overlapping region is used to extract the decay factor for the next cluster. This process is repeated for all clusters in the total PDP until the last cluster is reached. Note that the powers of overlapping rays are

calculated so that the total sum of the powers of overlapping rays corresponding to different clusters equals to the powers of the original total PDP. More details of this procedure is reported in [Erceg *et al.*, 2003].

Other auxiliary parameter is the number of MPCs that are within x dB of the peak amplitude, or the number of MPCs that carries at least y % of the total energy.

IV.2.7 Small Scale Fading

The distribution of the small-scale amplitudes is Nakagami [Zhang, 2002]

$$pdf(x) = \frac{2}{\Gamma(m)} \left(\frac{m}{\Omega}\right)^m x^{2m-1} \exp\left(-\frac{m}{\Omega} x^2\right) \quad (28)$$

where $m \geq \frac{1}{2}$ is the Nakagami m -factor, $\Gamma(m)$ is the gamma function, and Ω is the mean-square value of the amplitude. A conversion to a Rice distribution is approximately possible with the conversion equations

$$m = \frac{K_r + 1}{2} \quad (29)$$

$$\text{and} \quad K_r = \frac{\sqrt{m^2 - m}}{m - \sqrt{m^2 - m}} \quad (30)$$

where K and m are the Rice factor and Nakagami- m factor respectively.

The parameter Ω corresponds to the mean power, and its delay dependence is thus given by the power delay profile above. The m -parameter is modeled as a lognormally distributed random variable, whose logarithm has a mean μ_m and standard deviation σ_m .

Both of these can have delay dependence

$$\mu_m(\tau) = m_0 - k_m \tau \quad (31)$$

$$\text{and} \quad \sigma_m(\tau) = \hat{m}_0 - \hat{k}_m \tau \quad (32)$$

For the first component of each cluster, the Nakagami factor is modeled differently. It is assumed to be deterministic and independent of delay, where $m = \tilde{m}_0$.

IV.2.8 Generation of impulse response

Here it explains briefly the procedure for generating the impulse response for the designed Statistical Model step by step:

- 1) Generate a Poisson-distributed random variable L with mean \bar{L} . This is the number of clusters for the considered realization
- 2) Create $L - 1$ exponentially distributed variables x_n with decay constant Λ .
- 3) For each cluster, generate the cluster decay time using equation 23 and the total cluster power using equation 24.

- 4) For each cluster, generate a number of exponentially distributed variables x_n , from which the arrival times of the paths can be obtained. The actual number of considered components depends on the required dynamic range of the model.
- 5) For each component, compute the mean power using equation 22.
- 6) For the NLOS, compute the mean power using equation 25.
- 7) For each first component of the cluster, set the m-factor to m_0
- 8) For all other components, compute the mean and the variance of the m-factor using equations 31 and 32 respectively.
- 9) For each component, compute the realization of the amplitude as Nakagami-distributed variable with mean-square given by the mean power of the components as calculated in above steps.

Note: From the Saleh Valenzuela model, in last paragraph of section VII it explains that the amplitude of each ray is Rayleigh (or can be Nakagami which is used in this work or even Rician) because a 'ray' is sum of many independent signal replicas arriving within the time resolution of the receiver.

- 10) Compute phase for each component as uniformly distributed.
- 11) Make sure that the above description results in a profile that has AVERAGE power 1, i.e. when averaged over all the random processes.
- 12) For the simulation of the actual system, multiply the transfer function of the channel with the frequency-dependent transfer function of the channel and then to the frequency-dependent pathloss and emission spectrum.

Note: Channel transfer function is the Fourier transform for the generated impulse response.

$$P_{TX-amp}(f) \cdot \eta_{TX-ant}(f) \eta_{RX-ant}(f) \frac{PL_0}{\left(\frac{d}{d_0}\right)^2 \left(\frac{f}{f_c}\right)^2} \quad (33)$$

IV.3 Deterministic Model

This model was specifically designed for the second floor of the Applied Physics building, CICESE [Saul, 2005] for WIFI network. This model was modified by changing operating frequency to 2.4GHz, simulating it for receiving power upto -90 dBm, changed number of reflections and the location of transmitter and receivers in order to be able to use for WSN. These changes were made in the model because in case of WSN the transmitting power is too low and hence less number of multi trajectory reflections, the frequency band they work is different and finally was simulated according to the coverage required depending on the sensitivity of the receivers. It is based on C++ simulation and JAVA interface, in order to give the detailed graphical presentation for the coverage for a sensor or group of them; it also gives the power distribution on the entire floor.

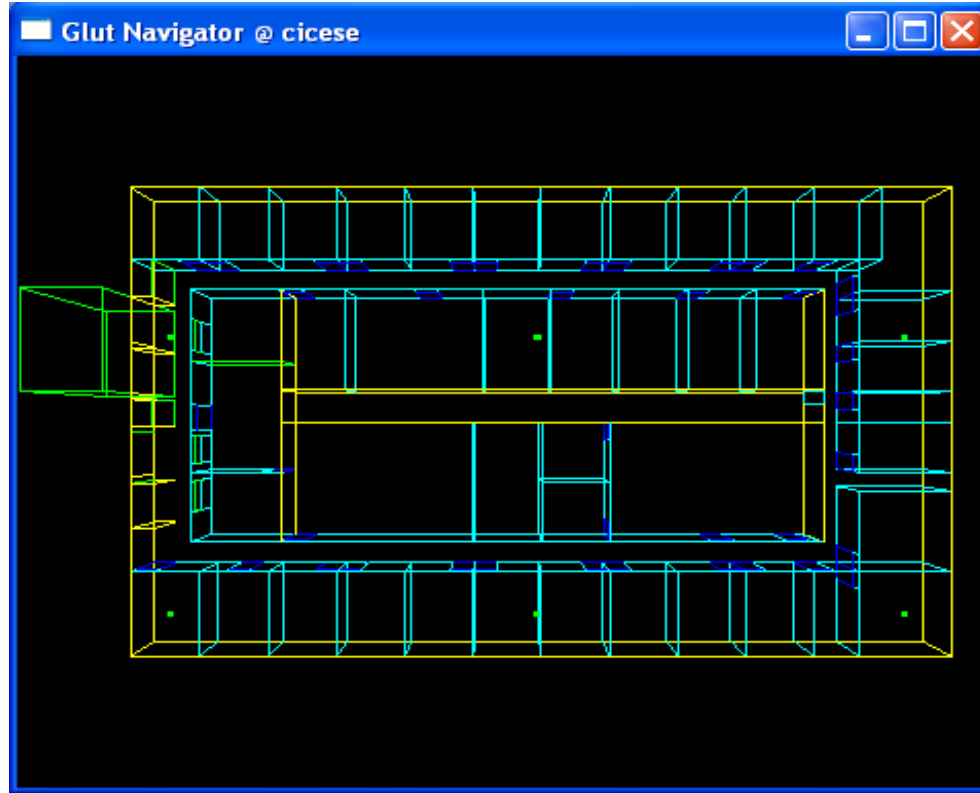


Figure 10: Basic Structure of Second floor, Applied Physics, CICESE.

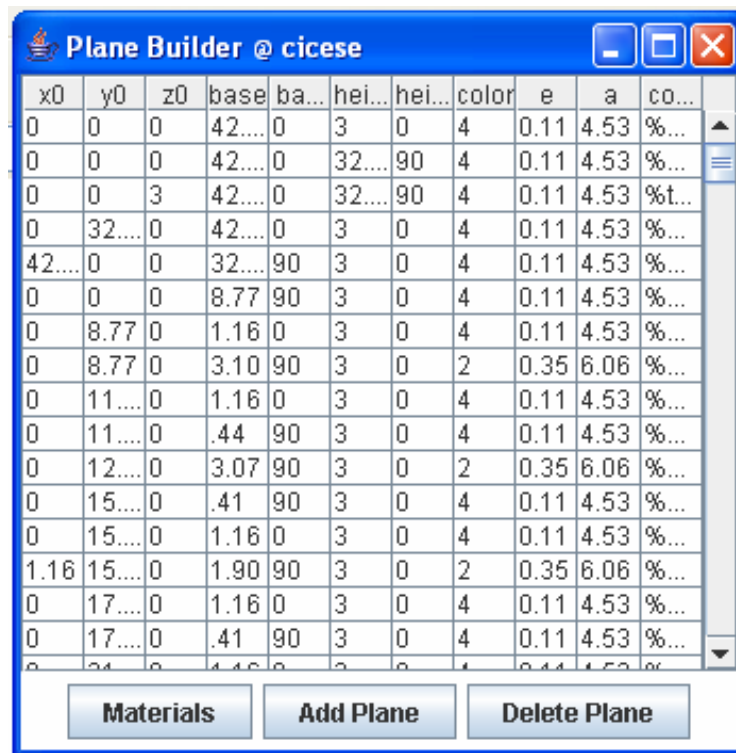
Figura 10: Estructura básica del segundo piso, Física Aplicada, CICESE.

Figure 10 represents the architectural structure of the experimental location that is the second floor, Applied Physics building, CICESE. As we can notice has many small rooms for offices and big halls for laboratory.

IV.3.1 Designing of the Model

This section presents the various steps and considerations involve in designing of a Deterministic Model.

- 1) Measurement for the entire second floor for Applied Physics building was taken, including every window, doors, metal racks, stairs, walls, etc. and a database of it was formed.
- 2) Then database of all the different types of material contained on the floor were listed along with their electric conductivity and dielectric permeability like wood, glass, etc.



x0	y0	z0	base	ba...	hei...	hei...	color	e	a	co...
0	0	0	42...	0	3	0	4	0.11	4.53	%...
0	0	0	42...	0	32...	90	4	0.11	4.53	%...
0	0	3	42...	0	32...	90	4	0.11	4.53	%t...
0	32...	0	42...	0	3	0	4	0.11	4.53	%...
42...	0	0	32...	90	3	0	4	0.11	4.53	%...
0	0	0	8.77	90	3	0	4	0.11	4.53	%...
0	8.77	0	1.16	0	3	0	4	0.11	4.53	%...
0	8.77	0	3.10	90	3	0	2	0.35	6.06	%...
0	11...	0	1.16	0	3	0	4	0.11	4.53	%...
0	11...	0	.44	90	3	0	4	0.11	4.53	%...
0	12...	0	3.07	90	3	0	2	0.35	6.06	%...
0	15...	0	.41	90	3	0	4	0.11	4.53	%...
0	15...	0	1.16	0	3	0	4	0.11	4.53	%...
1.16	15...	0	1.90	90	3	0	2	0.35	6.06	%...
0	17...	0	1.16	0	3	0	4	0.11	4.53	%...
0	17...	0	.41	90	3	0	4	0.11	4.53	%...
0	24...	0	4.46	0	0	0	4	0.44	4.53	%...

Figure 11: Database for various materials with corresponding size

Figura 11: Base de datos para varios materiales con el tamaño correspondiente

JAVA interface for the database of various materials in the building with the distance measurements with respect to all three axes, their size and their dielectric permittivity and electric conductivity is presented in figure 11.

- 3) The floor was divided into grids in order to facilitate programming for the coverage and power measurements as could be observed in figure 12 as well as also facilitates the physical measurements

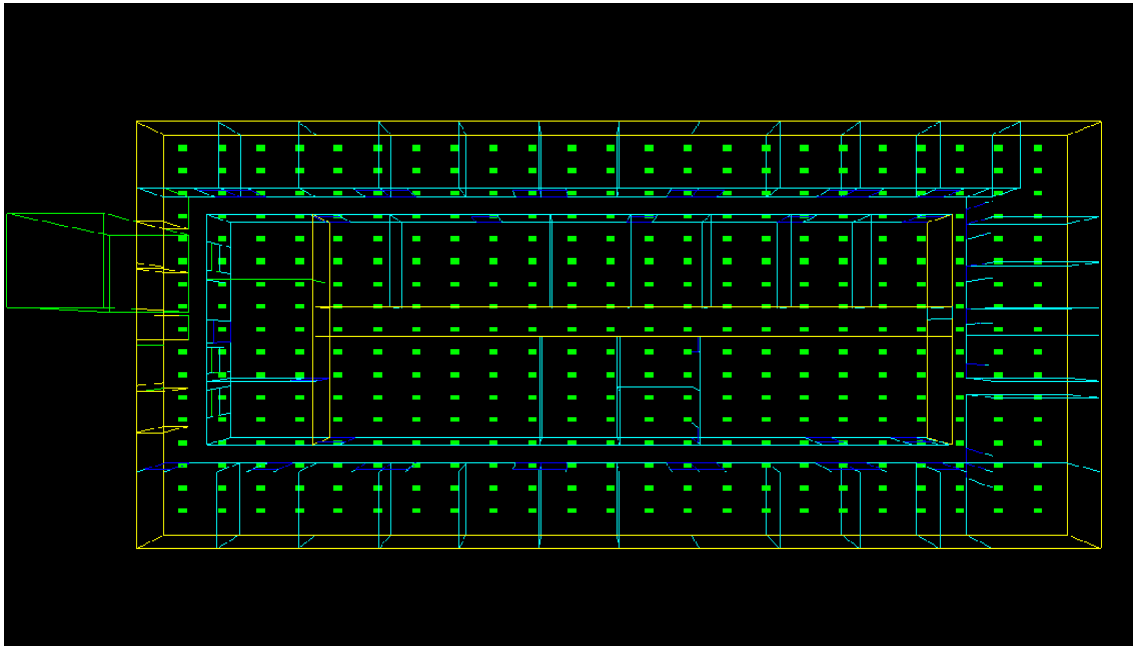


Figure 12: Grid Structure of the Applied Physics Building Second floor

Figura 12: Estructura de celdas para el segundo piso del edificio de Física Aplicada

- 4) C++ program was developed in order to simulate the coverage and power for the node or a combination of nodes.

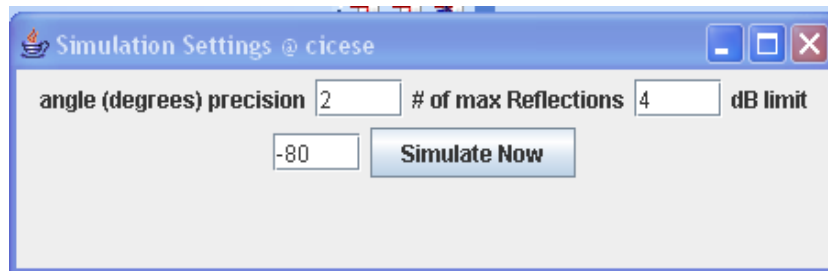


Figure 13: Java interface for the Simulation.

Figura 13: Interfase de Java para simulación.

- 5) This JAVA application simulation is based on the Number of nodes involved, number of reflections, angle precision, power limit and position of the nodes as can be seen in figure 13 and 14.

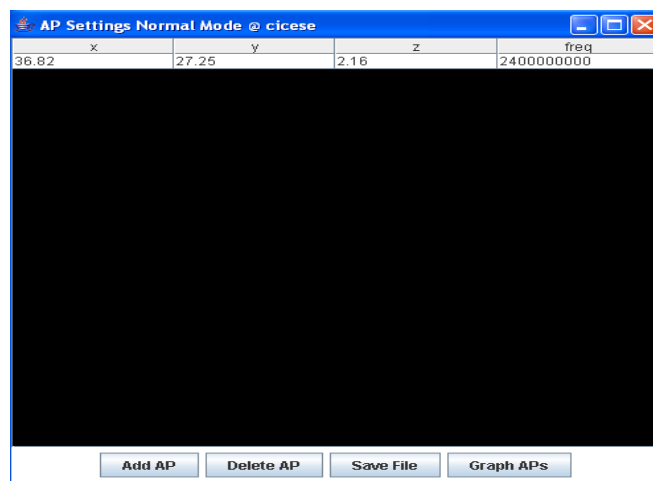


Figure 14: Java interface for addition of more sensors and changing location.

Figura 14: Interfase Java para agregar más sensores y cambiar posiciones.

- 6) Finally this simulation provides with graphical representation for the coverage and power distribution for different combinations of nodes as could be seen in the figure 15. The colored part presents the coverage and change in colors present power variation.

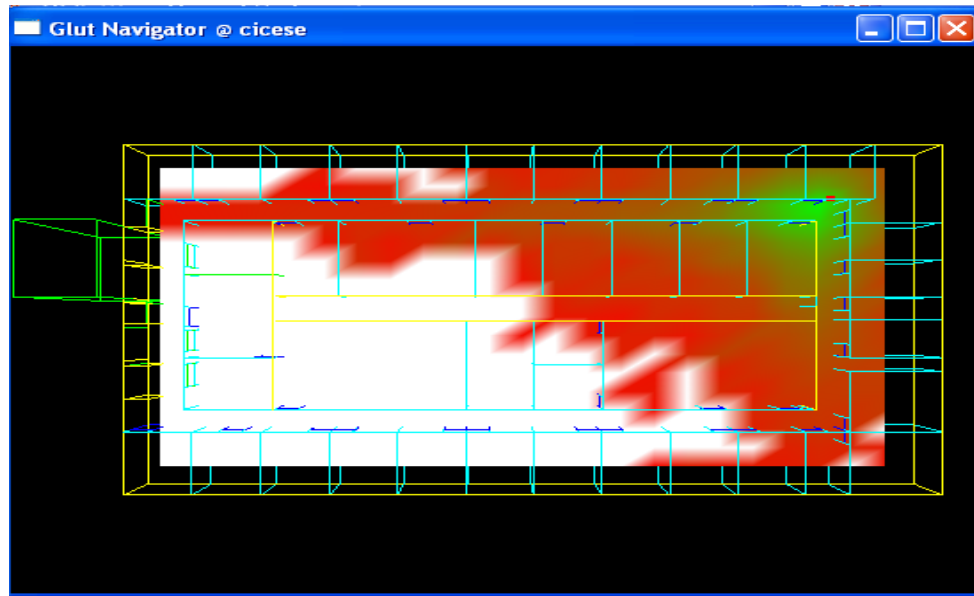


Figure 15: Graphical representation of the simulation result for coverage and Power profile.

Figura 15: Representación gráfica del resultado de la simulación de la cobertura y perfil de potencia

- 7) With this Java interface, the user can change all the following in order to achieve the desired output:
- 1) Location of node(s)
 - 2) Number of reflections
 - 3) Angle precision
 - 4) Power limit

- 5) Add or remove material along with dielectric permeability and electric conductivity.
- 6) Add new structure on the floor
- 7) Can program for entirely different location, changing the database for a new one.

Chapter V

Measurement and Result Analysis

V.1 Introduction

This chapter discusses and analyzes various results from the statistical model, deterministic model and physical measurements using sky tmote sensors. The work done could be basically divided into three categories, first the work done using Mote sensors, second the MATLAB results from the designed statistical model, and third the results of coverage and power distribution in case of deterministic model.

V.2 Work done on Sky tmote sensors

This section provides the detailed information about the various measurements and programming of the tmote sensors which were further implemented in the designing process of the radio channel model.

V.2.1 Programming of motes

The programmed tmote sensors provided with the basic network details and the sensor reading like the network topology, link quality indicator and AD (analog to digital) count.

1. Network topology: This part of the software provides with the details of the various nodes in the network and number of received and lost packets.

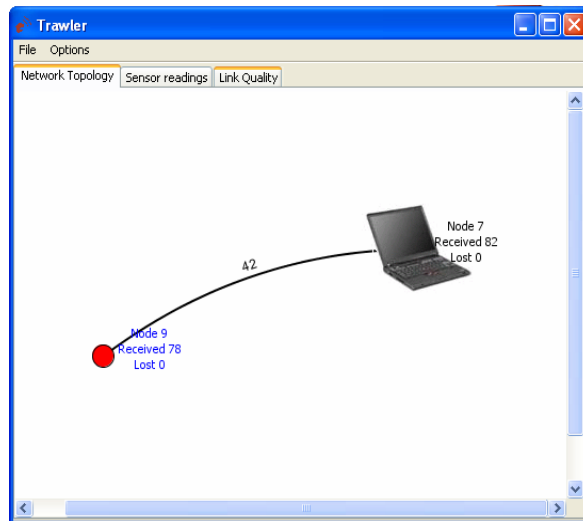


Figure 16: Network topology.

Figura 16: Topología de red.

2. Link quality indicator: This feature provides with the link quality between various nodes in the network.

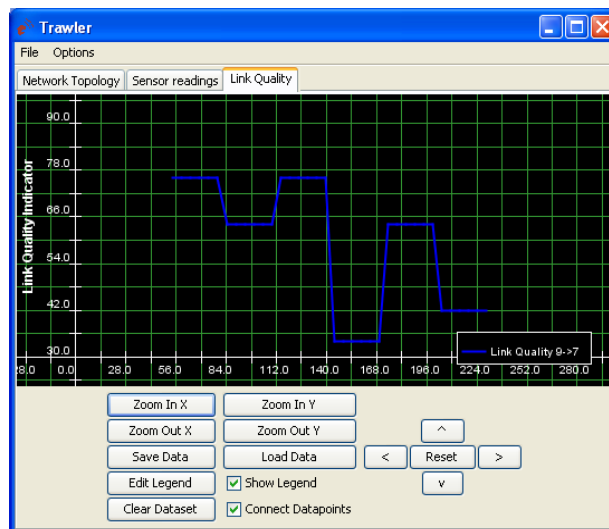


Figure 17: Link Quality Indicator.

Figura 17: Indicador de calidad de enlace.

3. AD count: ADC value provides with the sensor readings which correspond to the realistic temperature, humidity or light values depending on the type of sensor used by the node. These ADC values are related to realistic values by different formulas for temperature, humidity, etc.

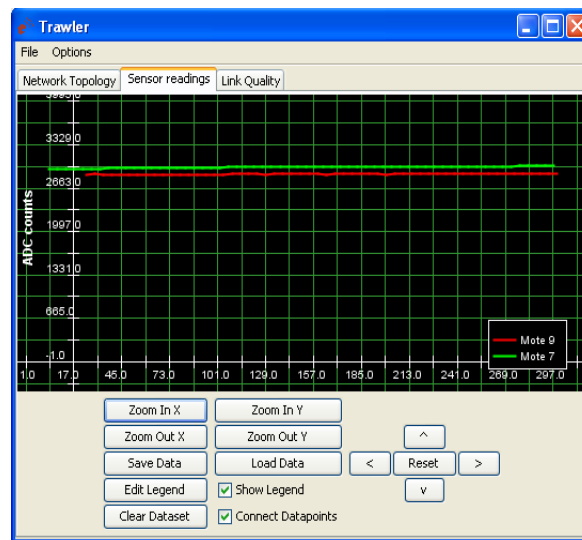


Figure 18: ADC count display.

Figura 18: Mostrador de cuenta ADC.

V.2.2 JAVA program

The original Sky mote sensor software only gives the readings for the Network Topology, Link quality indicator and the ADC counts; it doesn't give the final reading from respective sensors for temperature, humidity and light which are related to the value of ADC counts in certain form. So in order to make it more users friendly, a JAVA program was developed to give the reading for the respective sensors and show their connectivity details (thesis from Compute science department).

It can be observed from the figure 19 that there are four sensors connected in the network and duration they been connected. It can be seen that it also provides their respective sensor reading for light, humidity and temperature.

Fecha...	Nodo Id	Parent	Voltaje	Temper...	Humed...	Luz (PAR)	Luz (TS...	Temp Int	No Sec
4/12/07...	0	126	2.1899 V	27.22 C	37.621...	303.95...	31.860...	26.776 C	322
4/12/07...	3	0	2.2471 V	24.95 C	41.875...	421.14...	49.438...	22.030...	42
4/12/07...	2	0	2.2808 V	23.98 C	44.694...	369.87...	46.875...	18.420...	28
4/12/07...	1	0	2.2727 V	24.32 C	43.442...	285.64...	30.029...	24.093...	19

Lecturas

Figure 19: Java interface giving details for the different sensors connected in WSN, and the corresponding sensor readings.

Figura 19: Interfase Java dando detalles de los diferentes sensores conectados con WSN y sus lecturas respectivas.

V.2.3 Power Measurement

The next important issue was to be able to measure the received power from one sensor to another which was really not possible as the transmission in the case of sensors is not continuous, so to get the measurement for the power was not possible. Hence to solve this problem the motes were programmed to transmit continuously so one could take the measurements for the power using a 2.4 GHz spectrum analyzer. After taking various

reading on the second floor of applied physics building, CICESE, the average value of the readings was taken. The power range where the connectivity was maintained between two sensors varied from -59dBm to -87dBm , beyond -87dBm the power readings were still received until -91dBm but there was no connectivity between sensors. These measurements were taken at different hours of the day, when there were lot of people around and even when there were no people. But there were no separate readings taken for with and without people, just an average of all the readings were used. Another important point in these measurements is that the readings will vary from building to building depending on the constituting materials.

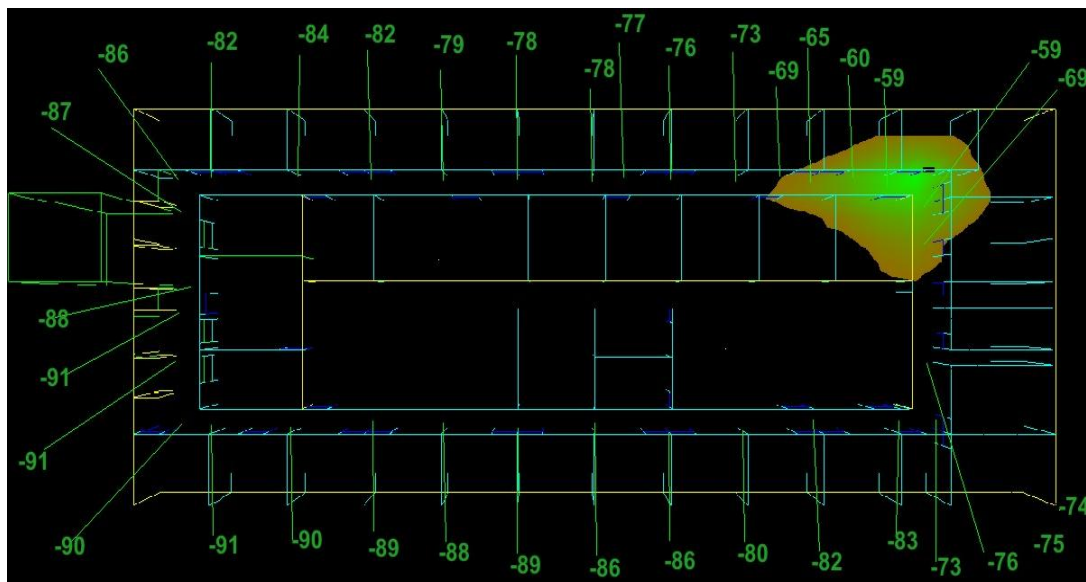


Figure 20: Received Power (dBm) measurement on the second floor of Applied Physics building, CICESE.

Figura 20: Mediciones de la potencia recibida (dBm) en el segundo piso del edificio de Física Aplicada, CICESE.

Figure 20 shows the power measurements for the second floor of the Applied Physics building as the fixed sensor and spectrum analyzer are placed at the top right corner of the building and moving the transmitting sensor to different locations.

Figure 21 shows the Power decay profile as a function of distance and it was observed that the power decay profile was in accordance to the theoretical assumptions.

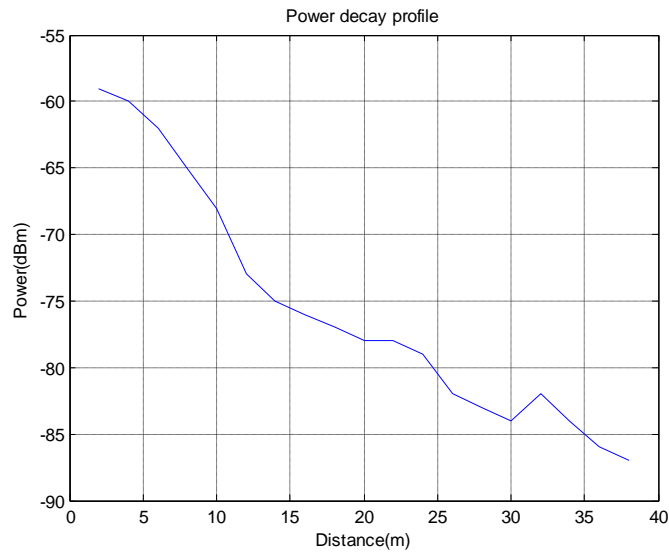


Figure 21: Received power (dBm) vs. distance (m).

Figura 21: Potencia recibida (dBm) vs. distancia (m).

V.3 Statistical Model Results

The previous chapter presented the designing of statistical model and the various equations which lead to the model, determining the basic characteristics of the radio channel like the impulse response, excess delay, rms delay and the power decay for two different scenarios LOS (line of sight) and NLOS (non-LOS), and here in this section the obtained simulation results are presented.

V.3.1 Parameters

The previous chapter consists of the designing equations for the statistical model, which utilizes following parameters for obtaining the results for various radio channel phenomenon, like impulse response, excess delay, RMS delay and power decay profile in this case.

- PL_0 pathloss at 1m distance
- n pathloss exponent
- σ_s shadowing standard deviation
- A_{ant} antenna loss
- κ frequency dependence of the pathloss
- \bar{L} mean number of clusters
- Λ inter-cluster arrival rate
- $\lambda_1, \lambda_2, \beta$ ray arrival rates (mixed Poisson model parameters)
- Γ inter-cluster decay constant
- k_γ, γ_0 intra-cluster decay time constant parameters
- $\sigma_{cluster}$ cluster shadowing variance
- m_0, k_m , Nakagami m factor mean
- \hat{m}_0, \hat{k}_m , Nakagami m factor variance
- \tilde{m}_0 Nakagami m factor for strong components
- γ_{rise}, γ_1 and χ parameters for alternative PDP shape

V.3.1 Line of Sight (LOS)

In this case we have clear line of sight between the transmitter and receiver; the only obstacles possible are mobile objects, for e.g. movement of people. Table 1 provides all the parameters that were used for indoor LOS scenario for matlab simulation. These parameter values have been taken from recognized work for indoor environment ([Kim *et al.*, 2004], [Molisch *et al.*, 2004]).

Table I: Parameters used for LOS scenario.
 Tabla I: Parámetros usados para escenario LOS.

	Indoor (LOS)
Pathloss	
N	1.63
σ_s	1.9
PL_0	36.6
A_{ant}	3dB
κ [Db/decade]	-3.5
Power delay profile	
\bar{L}	5.4
$\Lambda[1/ns]$	0.016
$\lambda_1, \lambda_2[1/ns], \beta$	0.19, 2.97, 0.0184
$\Gamma[ns]$	14.6
k_γ	0
$\gamma_0[ns]$	6.4
$\sigma_{cluster}[dB]$	NA
Small scale fading	
m_0	0.42dB
k_m	0
\hat{m}_0	0.31
\hat{k}_m	0
\tilde{m}_0	NA
χ	NA
γ_{rise}	NA
γ_1	NA

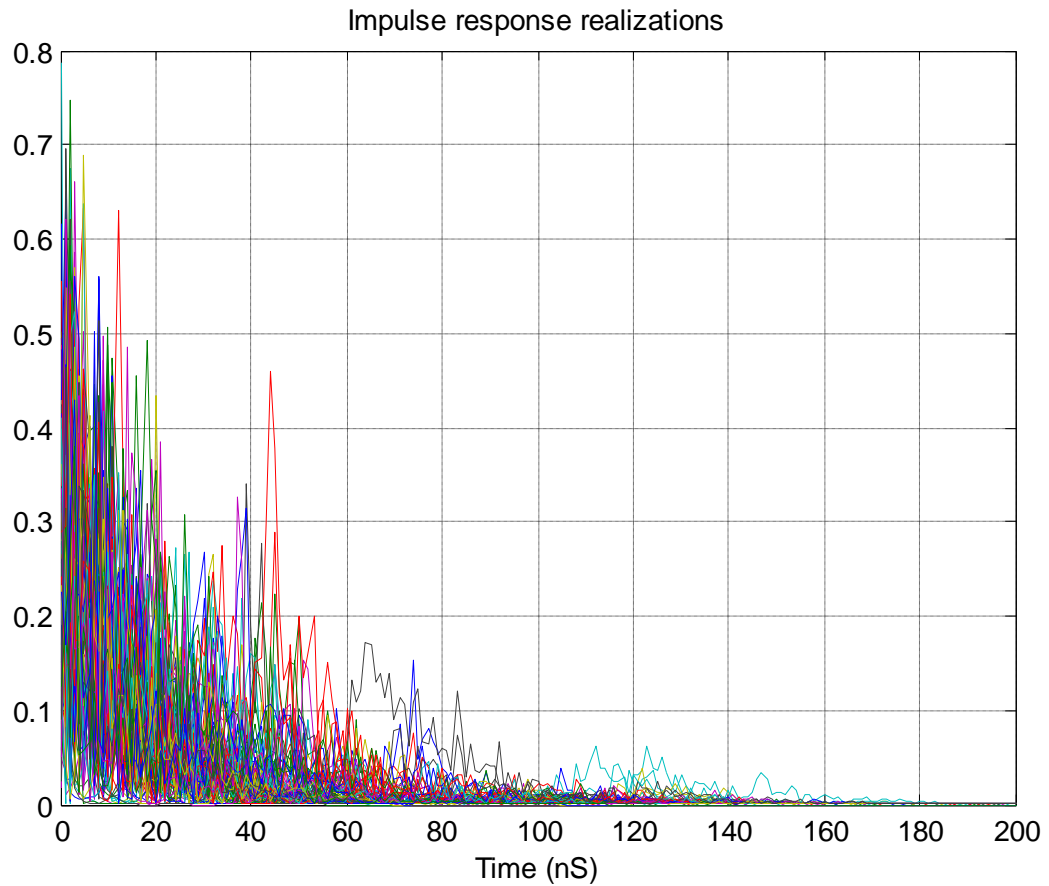


Figure 22: Impulse response vs. time for LOS scenario.

Figura 22: Respuesta al impulso vs. tiempo para escenario LOS

Figure 22 shows the impulse response of the radio channel as a function of time delay. The impulse response shows the arrival of clusters and rays within a cluster, it is observed that no ray arrives after 200ns, which is related to maximum delay spread. The impulse response for the LOS scenario is achieved from equation 18.

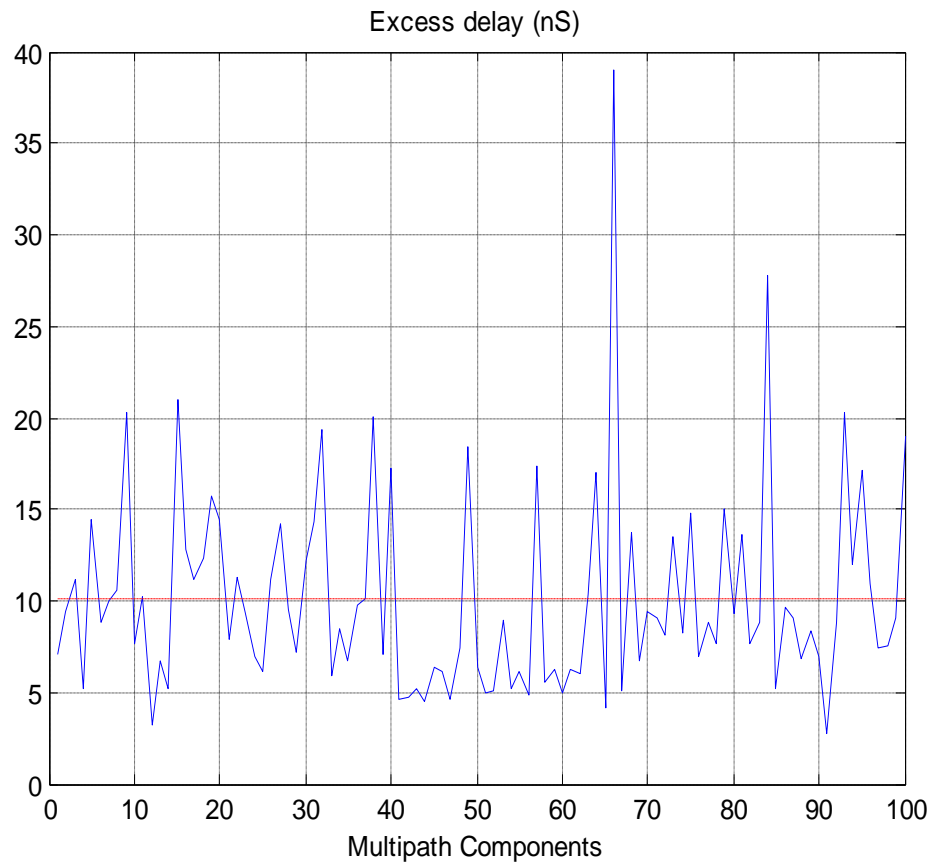


Figure 23: Excess delay with respect to Multipath components

Figura 23: Retardo en exceso con respecto a componentes multitrayectoria

Figure 23 shows the variation in the excess delay for different multipath components; was observed that the average excess delay is 10 ns. The huge peak at MPC 65-66 is due to multi reflection experienced by the signal. The excess delay can be calculated from the equation 26.

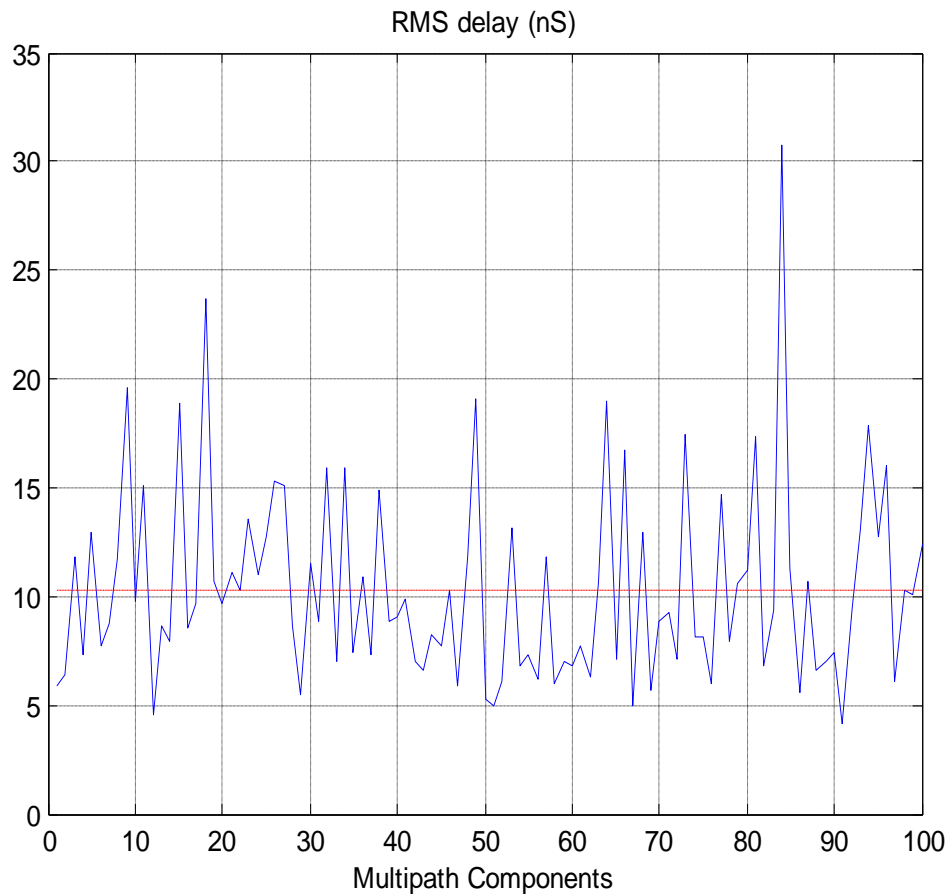


Figure 24: RMS delay for Multipath components

Figura 24: Retraso RMS para componentes multitrayectoria

Figure 24 shows the variation in root mean square (RMS) delay as function of MPC. It is observed that the average RMS delay is 10-11 ns. The above figure for the rms delay spread is achieved from equation 27.

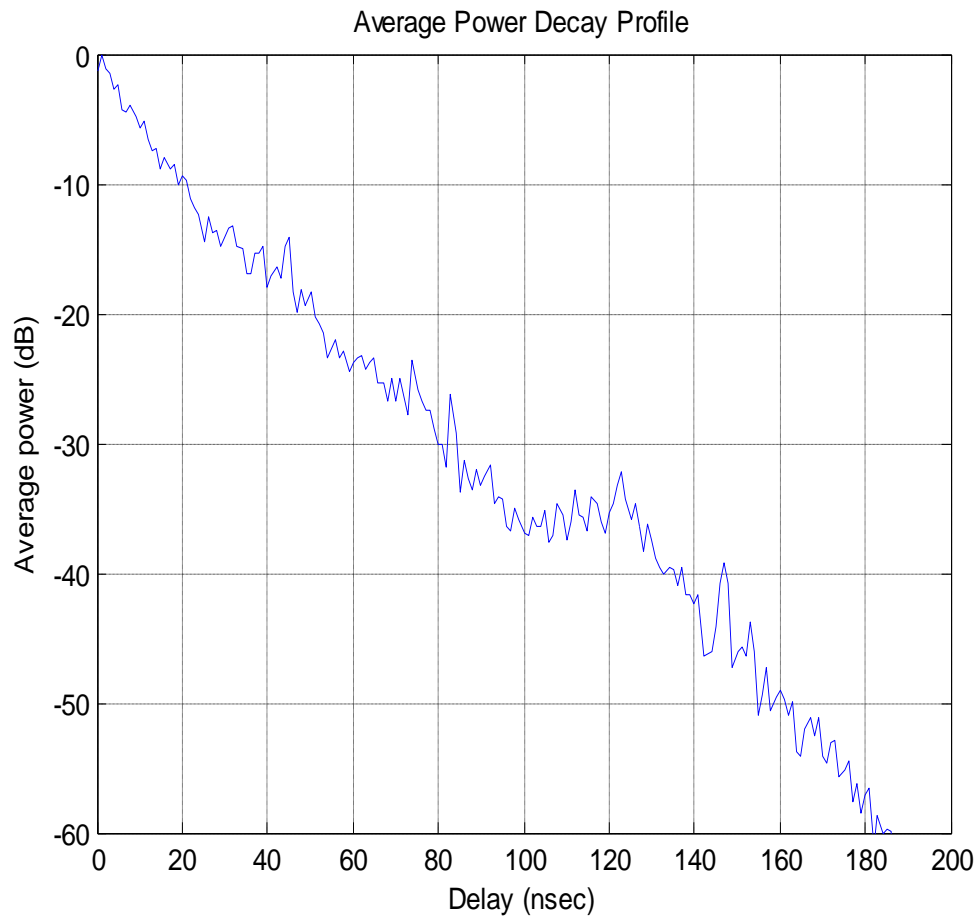


Figure 25: Average power decay profile.

Figura 25: Perfil de pérdida de potencia promedio

Figure 25 shows the average power decay profile as a function of the delay. In the figure 0 dBm is considered to be the maximum received power. The power decay profile along time has same behavior as with respect to distance, in both cases the power decay is exponential (figure 25 and figure 31). The power decay profile can be achieved from the equation 22.

V.3.2 No Line of Sight (NLOS)

In this scenario there is no direct line of sight between transmitter and the receiver, there are stationary obstacles in between, for e.g. walls, doors, etc. The following table provides with values of the parameters which are used for the NLOS scenario ([Kim *et al.*, 2004], [Molisch *et al.*, 2004]).

Table II: Parameters used for NLOS scenario

Tabla II: Parámetros usados para escenario NLOS

	Indoor (NLOS)
Pathloss	
N	3.07
σ_s	3.9
PL_0	51.4
A_{ant}	3Db
κ [dB/decade]	5.3
Power delay profile	
\bar{L}	1
Λ [1/ns]	NA
λ_1, λ_2 [1/ns], β	NA
Γ [ns]	NA
k_γ	NA
γ_0 [ns]	NA
σ_{cluster} [dB]	NA
Small scale fading	
m_0	0.50dB
k_m	0
\hat{m}_0	0.25
\hat{k}_m	0
\tilde{m}_0	
χ	0.86
γ_{rise}	15.21
γ_1	11.84

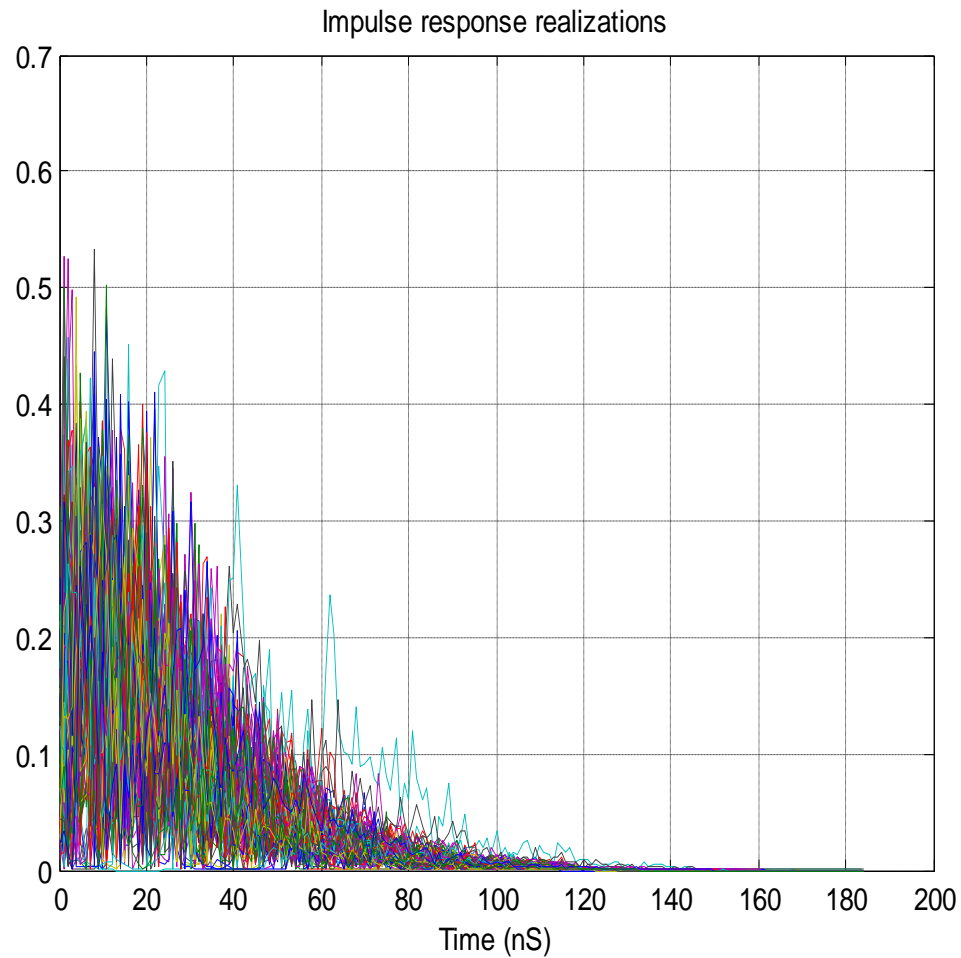


Figure 26: Impulse response for the NLOS scenario vs. Time.

Figura 26: Respuesta al impulso para escenario NLOS vs. Tiempo.

Figure 26 shows the impulse response of the radio channel as a function of time delay for NLOS scenario. Impulse response shows the arrival of clusters and rays within a cluster. Comparing above result with LOS impulse response it can be observed that the received signals are stronger and lasts longer in LOS. The above figure is obtained from equation 18.

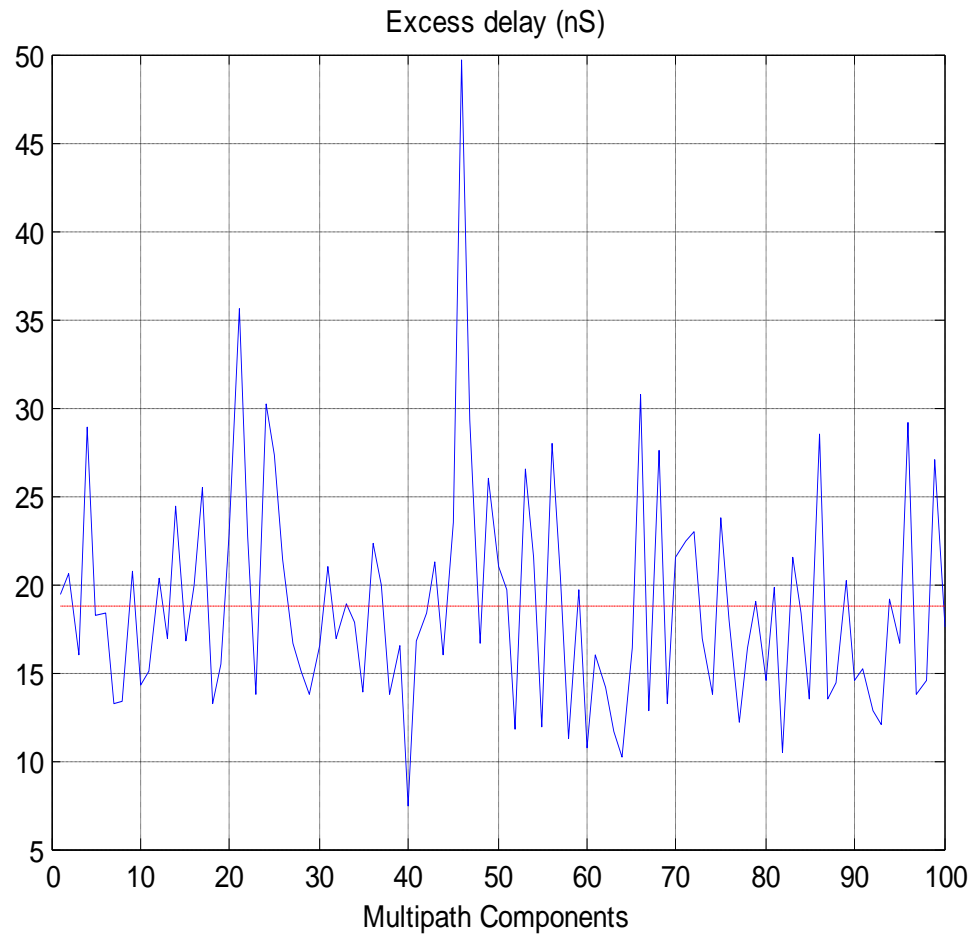


Figure 27: Excess delay for different Multipath components.

Figura 27: Retardo en exceso para diferentes componentes multitrayectoria.

Figure 27 shows the variation in the excess delay for different multipath components; comparing the above result with LOS scenario it can be observed that in case of NLOS the average excess delay raises to 19ns. This can be explained for the multiple reflections experienced by the signal due to no clear line of sight because of the obstacles present. The above figure is obtained from equation 26.

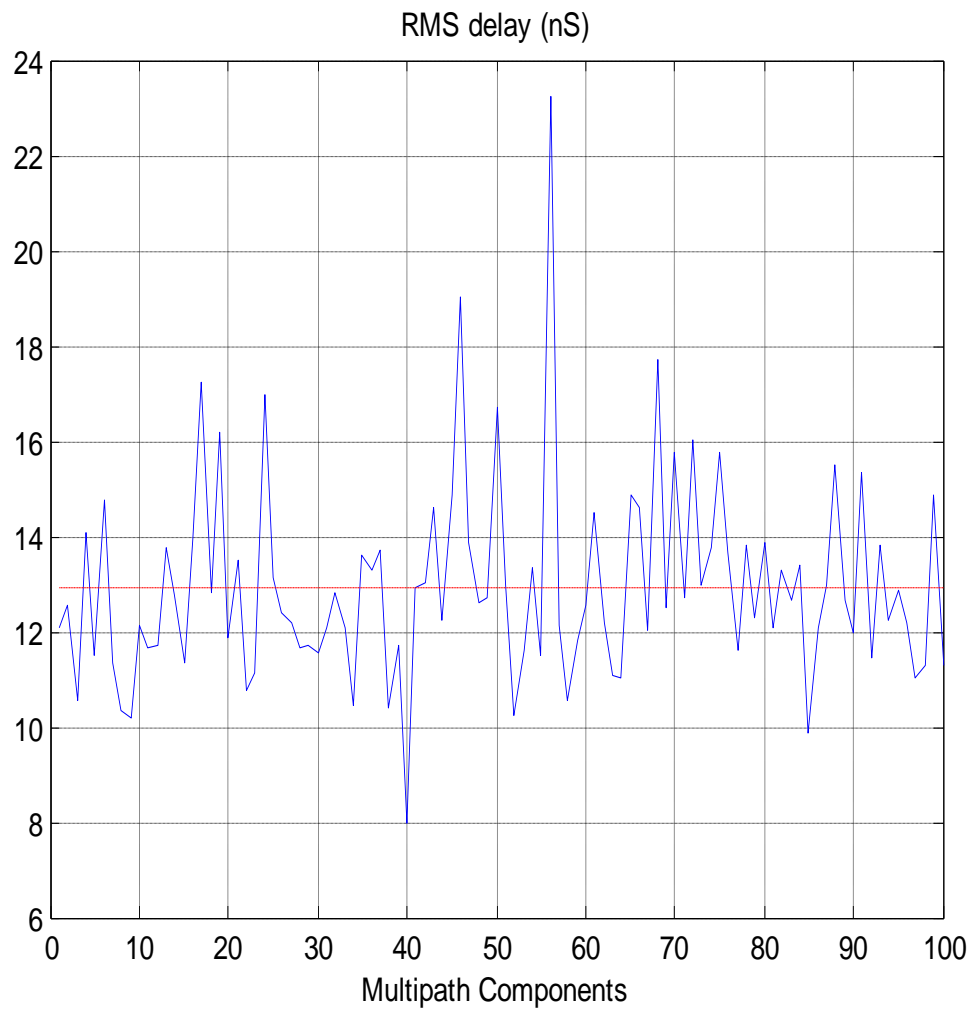


Figure 28: RMS delay for multipath components.

Figura 28: Retraso RMS para componentes multitrayectoria.

Figure 28 shows the variation in root mean square (RMS) delay as function of MPC. It is observed that the average RMS delay is 13 ns, higher than the LOS scenario. The figure 28 is obtained from equation 27.

Figure 29 shows the average power decay profile as a function of the delay. In the figure below, 0 dBm is considered to be the maximum received power. Comparing to LOS scenario we see that the power decay is faster in NLOS scenario. The figure of power profile below is obtained from equation 25.

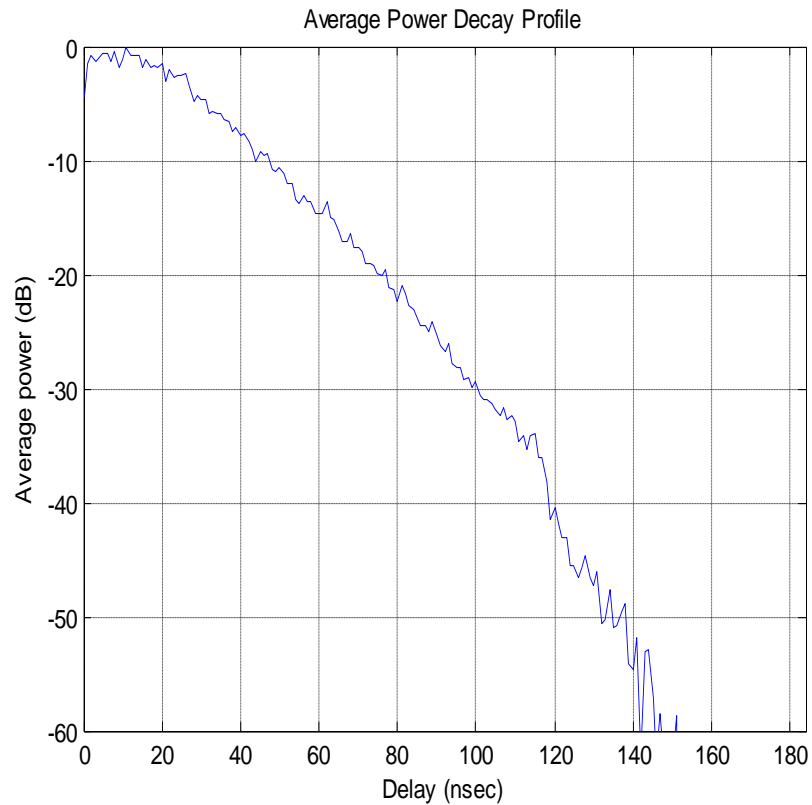


Figure 29: Power decay profile for the NLOS scenario.

Figura 29: Perfil de pérdida de potencia para escenario NLOS.

Up to this point the basic matlab results for the designed radio channel model have been presented (for wireless sensor networks). There are other auxiliary parameters which can be generated using this matlab simulation like the desired power components, percent of components above particular power level, etc.

V.4 Deterministic Model

As its been already explained, this model was specifically designed for the second floor of Applied Physics building, CICESE, since all the physical measurements have been taken for this floor including the doors, windows, walls, stairs and other structures, considering each materials permittivity and conductivity like for brick, glass, wood, etc. Through the use of this model one can achieve the best combination (having different locations on floor) using minimum number of sensors, to achieve full coverage for the floor. This section presents two important results of this model the Power Measurement and the coverage for a pair of sensor.

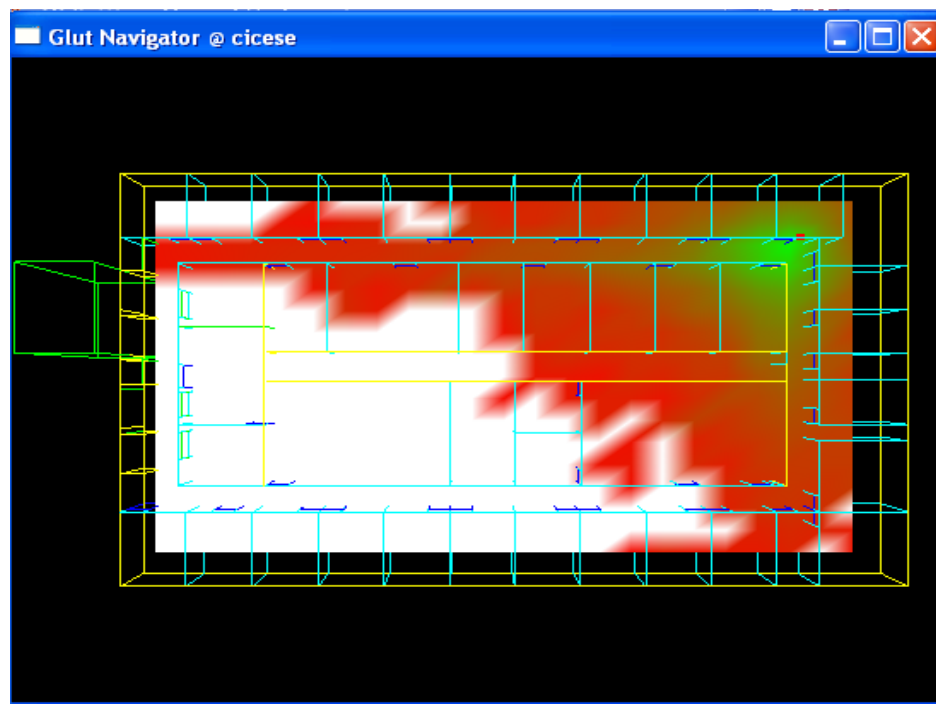


Figure 30: Coverage and the power variation for second floor.

Figura 30: Cobertura y variación de potencia para el segundo piso.

Figure 30 shows the coverage of the mote located on the top right of the figure and power variation represented by variation in the color (green: stronger, red: weaker).

Figure 31 shows power decay with the change in the distance, as obtained through deterministic model. It is observed that the power decay satisfies the theoretical as well as practical expectation.

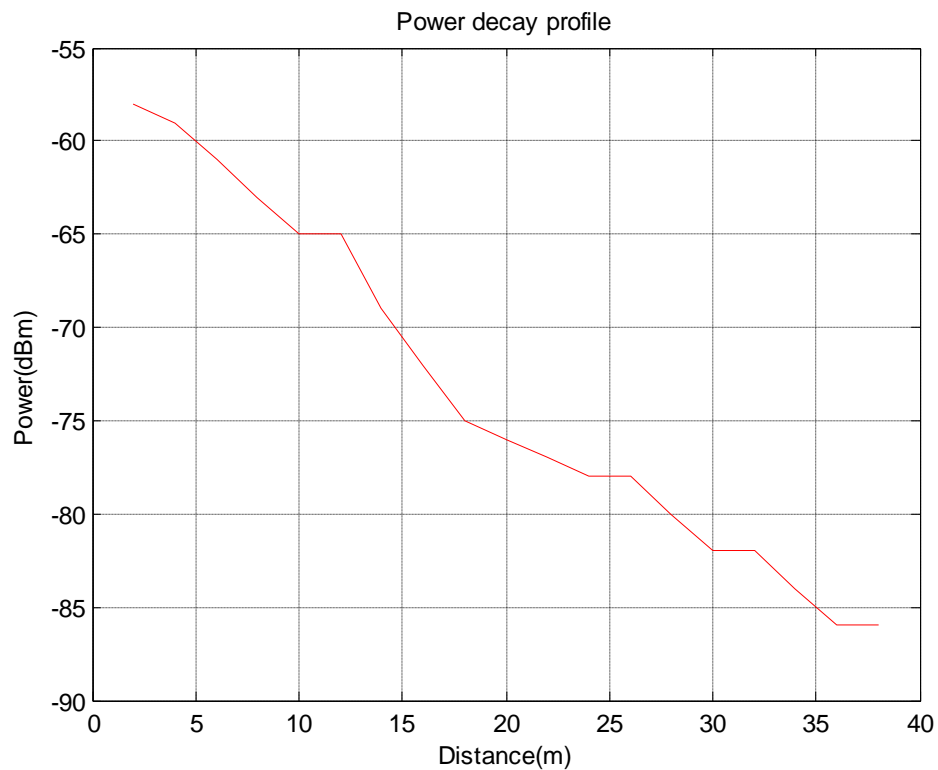


Figure 31: Power decay vs. distance

Figura 31: Pérdida de potencia vs. distancia

V.5 Result Analysis

As was mentioned before, three sets of results were obtained, the first with the statistical model, the second with deterministic model and third with physical measurements. This

section compares the results achieved on basis of two grounds, coverage and Power decay profile. The results obtained from the statistical model cannot be directly compared with another model as no other model exists for WSN for indoor environment, but compared to the physical measurements and deterministic model to understand radio channel (indoor environment) for WSN.

- 1) Coverage: When the results for the coverage from the deterministic model and the physical reading are compared it can be seen that the coverage for both of them is almost the same.

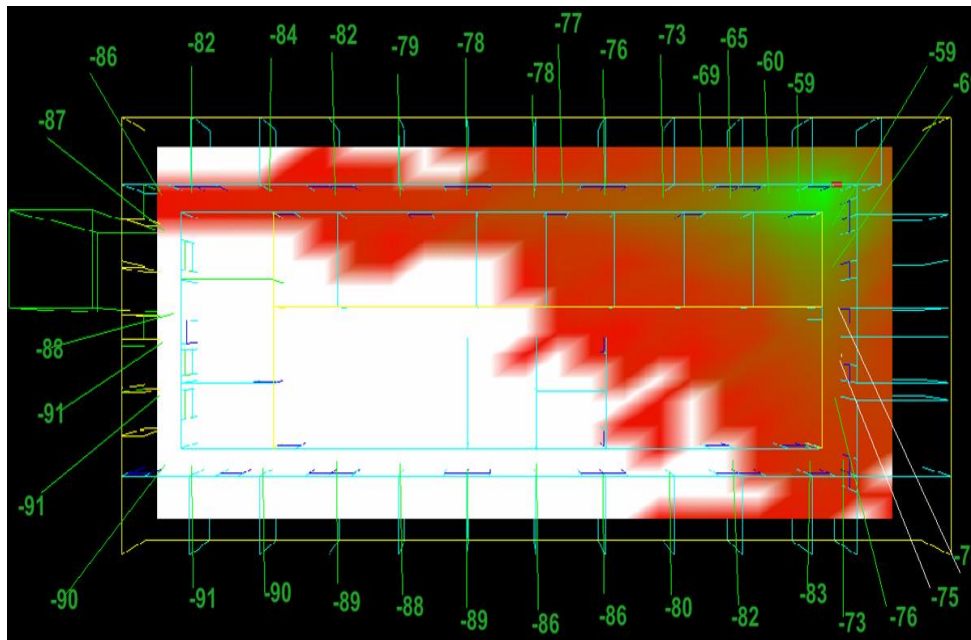


Figure 32: The coverage for the measured reading exits up to -87dBm , and the result of the coverage from deterministic model is on background in color.

Figura 32: La cobertura de las lecturas medidas llega hasta -87dBm , y el resultado de la cobertura con el modelo determinístico se muestra al fondo en color.

From figure 32, the measured power readings have coverage up to -87dBm (physical reading), above -87dBm there is no coverage and the result for coverage from the deterministic model is shown in the colored background.

- 2) Power decay: Comparing the results obtained from the deterministic model and the physical measurements, it can be observed that they have very similar power decay profile over distance as shown in figure 33. The results cannot be compared directly with the results from statistical model, as the power decay (figure 25) is function of time whereas in case of deterministic model and physical measurements power decay is function of distance.

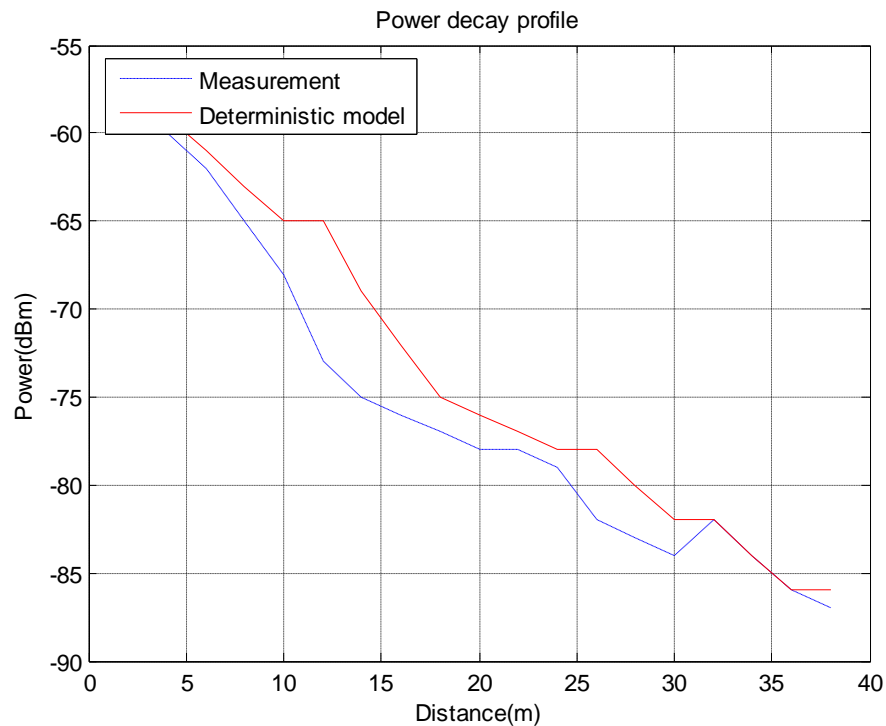


Figure 33: Power decay comparison for Physical measurements and Deterministic model output

Figura 33: Comparación de pérdida de potencia para medidas físicas y resultados del modelo determinístico

Chapter VI

Conclusions and Future Work

Earlier chapter IV presented the details of designed statistical radio channel model and deterministic radio channel model were explained and chapter V presented the results for these two radio channel model and the physical measurements taken on the second floor of the Applied Physics building and their analysis. This chapter presents conclusions from result analysis and other observations made during designing of the radio channel model, it also presents future work as well as major contribution of this thesis.

VI.1 Conclusions

The conclusions that were made from this work and analysis of results are as following:

- 1) The designed statistical model (inspired by Saleh Valenzuela model) for indoor environment WSN serves to characterize the radio channel behavior, and provides the basic radio channel parameters like power decay, impulse response, spread delay, rms delay.
- 2) The deterministic model really helps in knowing the coverage of motes placed at any part of the second floor of the Applied Physics building (CICESE) which can be beneficial in network planning and implementing routing algorithm. With this

model one can not only know the coverage but also the power distribution over the entire floor. It also gives the best coverage combinations depending on the number of Sensors one wants to use.

- 3) The Java interface for the Motes give the detailed information regarding the Sensor readings, link quality and network topology, which is very user friendly. As from original software, one gets the values in terms of ADC counts, which for a non expert is hard to comprehend, but with this JAVA application any one can virtually see the change in temperature, humidity, light intensity, etc.
- 4) The physical measurements taken for the coverage of the sensor on the second floor of the Applied Physics building are very similar to the output of the deterministic radio channel model. With average of series of measurements, it was seen that the coverage results achieved comply with the output of deterministic model.
- 5) The indoor channel is quasi-static or very slowly time varying and suffers attenuation by the people's movement. During physical measurements it could be observed that under the presence of mobile obstacles there was random signal attenuation.

- 6) It was observed during measurements that the nature and statistics of the channel's impulse response is virtually independent of the states of polarization of the transmitting and receiving antennas (not valid for no line-of-sight).
- 7) The power decay profile for the deterministic model and the physical measurements are very alike and this verifies the validity of the deterministic model (Fig. 33).
- 8) The Statistical model is based on a mixture of two Poisson processes and gives an excellent match to the ray arrival times with respect to the single Poisson process proposed in the original S-V model.

VI.2 Future Work

There are many ways in which this work could be extended, but few of the most important ones are as following:

- 1) As this is the first statistical radio channel model for Wireless sensor network for indoor environment, still one can modify this model in order to design it for another environments, for e.g. outdoor environment, industrial environment, etc. For other environments the manner for defining the model could remain the same but the values for the used parameters would vary and hence measurements should be taken again.

- 2) Due to lack of the specialized laboratory equipment there were few limitations in the radio channel model implementation, as for instance it was not possible to compare few results of the designed model with physical measurements. For example non availability of vector channel sounder, which produces periodic multifrequency test signal. Hence using a well equipped laboratory can help in improvising few parameters in the radio channel model.

VI.3 Major Contributions

Major Contributions of this thesis can be considered as proposing a radio channel model for Wireless Sensor Network, for indoor environment. This model covers all basic parameters involved in description of a radio channel. Besides, the physical measurements provide with coverage, power decay and network topology details for a sensor, which helps in implementation of wireless sensor network for the second floor of applied physics building, CICESE. Finally, with the help of deterministic model can achieve complete details for coverage and power profile for the implemented WSN.

References

- Boutin, M. Affes, S. Despins, C. and Denidni, T. 2005. "Statistical modeling of a radio propagation channel in an underground mine at 2.4 and 5.8 GHz" *Vehicular Technology Conference, 2005. VTC 2005-Spring. 2005 IEEE 61st.* 1(1): 78- 81p
- Chong C. C., Tan, C. M., Laurenson, D. I., McLaughlin, S., Beach, M. A., Nix, A. R. 2003. "A New Statistical Wideband Spatio-Temporal Channel Model for 5-GHz Band WLAN Systems," *IEEE J. Select. Areas Commun.*, 21(2): 139-149 p.
- Erceg V., L. Schumacher, P. Kyritsi, D. S. Baum, A. F. Molisch, and A. Y. Gorokhov. 2003. "Indoor MIMO WLAN channel models," In Standardization drafts of IEEE 802 meeting Dallas, March 2003.
- Ganesh R., Pahlavan K. 1991. "Statistical modeling and computer simulation of indoor radio channel", *IEEE Proceedings-I*, 138(3):153-161p.
- Gang Z., T. He, S. Krishnamurthy and John A. Stankovic, University of Virginia. 2006. *ACM Transactions of Sensor Networks*, 2(2): 221-261p.
- Hashemi H. 1993. "Impulse response modeling of indoor radio propagation channels", *IEEE Journal on Selected Areas in Communications*, 11(7):967-978p.
- Hassan-Ali M., Pahlavan K., 2002. "A new statistical model for site-specific indoor radio propagation prediction based on geometric optics and geometry probability", *IEEE transactions on wireless communications*, 1(1):112-124p.
- Hashemi H, Tholl D., 1994. "Statistical Modeling and Simulation of the RMS Delay Spread of Indoor Radio Propagation Channels", *IEEE Transactions on vehicular technology*", 43(1):110-120p.
- Hashemi H., 1979. "Simulation of the urban radio propagation channel", *IEEE transactions on VT*, VT28(3): 213-225.
- J. Karedal, S. Wyne, P. Almers, F. Tufvesson, A. F. Molisch, 2004. "Statistical analysis of the UWB channel in an industrial environment" *IEEE Vehicular Technology Conference (VTC)*, 1: 81-85p.
- G. Kadel and R. Lorenz, 1995. "Impact of the radio channel on the performance of digital mobile communication systems," in *Sixth IEEE Int. Symp. on Personal, Indoor and Mobile Radio Communications PIMRC'95*, Toronto, Ont., Canada, 27-29 Sep 1995. 2(2):419-423p.

- C. Liu, E. Skafidas, T.S. Pollock and R.J. Evans, 2006. "Angle of arrival extended S-V model for the 60 GHz wireless desktop channel" in *Seventeenth IEEE Int. Symp. on Personal, Indoor and Mobile Radio Communications PIMRC'06*, Helsinki, Sept 2006.
- Litva J., Wu C., Ghaforian A., 1996. "Use of FDTD for simulating the angle of arrival and time delay of signals propagating in indoor environments", *IEEE Electronics Letters*, 32(10).
- F.L. Lewis, "Wireless Sensor Networks" 1-18p. In Ed. D.J. Cook and S.K. Das, John Wiley, *Smart Environments: Technologies, Protocols, and Applications* New York, 2004.
- A. F. Molisch, K. Balakrishnan, C. C. Chong, S. Emami, A. Fort, J. Karedal, J. Kunisch, H. Schantz, U. Schuster, K. Siwiak, 2005 "IEEE 802.15.4a channel model - final report" *IEEE* 2004. 63p.
- J.O. Nielsen, G. F. Pedersen, K. O. K, and I. Z. K. I.Z, 2001. "Statistics of measured body loss for mobile phones", *Antennas and Propagation, IEEE Transactions on* 49(9):1351–1353p.
- R. Qiu and I.-T. Lu, 1996. "Wideband wireless multipath channel modeling with path frequency dependence," in *IEEE International Conference on Communications (ICC'96)*. Dallas, TX, USA, 23-27 Jun 1996 1(1): 277-281p.
- Rappaport T. S., Seidel S. Y., Takamizawa K., 1991. "Statistical channel impulse response models for factory and open plan building radio communication system design", *IEEE Transactions on Communications*, 39(5):794-807.
- J.-P. Rossi, 1999. "Influence of measurement conditions on the evaluation of some radio channel parameters," *IEEE Trans. on Vehicular Technology*, VT48:1304–1316p.
- Saleh A.M, Valenzuela R. A., 1987. "A statistical model for indoor multipath propagation", *IEEE Journal on Selected Areas on Communications*, 5(2): 128 – 137p.
- P. Smulders, M. Jevrosimovic, M. Herben, S. Savov, E. Martijn. 2002, "State of the art channel models". In web page: http://www.brabantbreedband.nl/publications/BTS01063-BR@H-D21-PUB_channel%20models.pdf, Agosto 2006. 10-18p.
- Q. H. Spencer, B. D. Jeffs, M. A. Jensen, and A. L. Swindlehurst, 2000. "Modeling the statistical time and angle of arrival characteristics of an indoor multipath channel," 18: 347–360p.
- Simon L. Cotton, William G. Scanlon, 2006. "A statistical analysis of indoor multipath fading for a narrowband wireless body area network" in 17th Annual IEEE International Symposium on Personal, Indoor and Mobile Radio Communications (PIMRC'06). Helsinki, Sept. 2006. 1-5 p.

Shinsuke H., D. Zhao, K. Yanagihara, J. Taketsugu, 2005. "Propagation characteristics of IEEE 802.15.4 radio signal and their application for location estimation" in: Vehicular Technology Conference, 30 May-1 June 2005. VTC 2005-Spring. 2005 IEEE 61st 1(1): 97- 101.

S. C.Rochin, J. Sanchez "Wireless network design planner method", In reporting process. CICESE, 2005.

Tmote Sky Data Sheet. www.moteiv.com. 2007.

G. L. Turin, F. D. Capp, T. L. Johnson, S. B. Fine, and D. Lavry, 1972. "A statistical model of urban multipath propagation," *IEEE Trans. Veh. Technol.*, VT21:1-9p.

Tadeuz A. Wysocki and Hans –Jurgen Zepernick, 2000. "Characterization of the indoor radio propagation channel at 2.4GHz" in Journal of telecommunications and information technology, 3-4.

U.C.A.N., 2003. "Report on UWB basic transmission loss," Tech. Rep. IST-2001-32710, IST-2001-32710.

Q. T. Zhang, 2002. "A note on the estimation of Nakagami-m fading parameter," *Communications Letters, IEEE*. 6(6):237 – 238p.